TU Delft

Delft University of Technology

ESEM observation and rheological analysis of rejuvenated SBS modified bitumen

Lin, P.; Liu, X.; Apostolidis, P.; Erkens, S.; Zhang, Y. ; Ren, S.

DOI
10.1016/j.matdes.2021.109639

Publication date
2021

Document Version
Final published version

Published in
Materials & Design

Citation (APA)
Lin, P., Liu, X., Apostolidis, P., Erkens, S., Zhang, Y., & Ren, S. (2021). ESEM observation and rheological analysis of rejuvenated SBS modified bitumen. *Materials & Design*, *204*, 1-18. Article 109639. https://doi.org/10.1016/j.matdes.2021.109639

Important note
To cite this publication, please use the final published version (if applicable).
Please check the document version above.

Copyright
Other than for strictly personal use, it is not permitted to download, forward or distribute the text or part of it, without the consent of the author(s) and/or copyright holder(s), unless the work is under an open content license such as Creative Commons.

Takedown policy
Please contact us and provide details if you believe this document breaches copyrights.
We will remove access to the work immediately and investigate your claim.

This work is downloaded from Delft University of Technology.
For technical reasons the number of authors shown on this cover page is limited to a maximum of 10.

Materials and Design 204 (2021) 109639

Contents lists available at ScienceDirect

Materials and Design

journal homepage: www.elsevier.com/locate/matdes

ESEM observation and rheological analysis of rejuvenated SBS modified bitumen

P. Lin [a,*], X. Liu [a], P. Apostolidis [a], S. Erkens [a], Y. Zhang [b], S. Ren [a]

[a] Civil Engineering and Geosciences, Delft University of Technology, Delft 2628CN, the Netherlands
[b] School of Highway, Chang'an University, Xi'an 710064, Shaanxi, China

HIGHLIGHTS

- The addition of rejuvenators contributes to the formation of fibril structure and increases the distance between fibrils.
- The influence of rejuvenator types/dosages on the fibril-structure can be demonstrated with ESEM.
- A process for extracting quantification parameters from the fibril-structure of bitumen is proposed.
- The fibril-structure parameters exhibited a significant correlation with rheological properties.

GRAPHICAL ABSTRACT

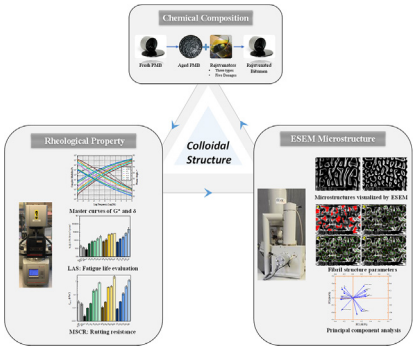

ARTICLE INFO

Article history:
Received 10 September 2020
Received in revised form 4 March 2021
Accepted 5 March 2021
Available online 08 March 2021

ABSTRACT

Observing the microstructure of bituminous binders with an environmental scanning electron microscope (ESEM) can contribute significantly to reveal the underlying rejuvenation mechanism. In this study, three rejuvenators were selected to regenerate the aged SBS modified binders at five dosages, and their rheology was evaluated using a dynamic shear rheometer. ESEM was employed to examine the microstructure of binders as well, and a series of microstructure parameters were quantified with image analysis. The results demonstrated that the chemical composition changes correspond to the evolution of microstructure morphological and rheological properties. Moreover, the rheological and microstructure characteristics were analyzed with Principal Component Analysis (PCA) and regression analysis. Based on PCA results, the microstructure of rejuvenated binders has shown a good correlation with stiffness after combining various principal components. According to regression analysis, the distance between adjacent fibrils exhibited a significant correlation with $J_{nr3.2}$ and the complex modulus index. Overall, the results of this study strengthen the hypothesis that the ESEM microstructure is intimately correlated with chemical composition and rheological properties, rather than with irrelevant surface phenomena.

Bitumen, polymer modified bitumen, rejuvenator, microstructure, rheology, environmental scanning electron microscopy.

© 2021 The Authors. Published by Elsevier Ltd. This is an open access article under the CC BY license (http://creativecommons.org/licenses/by/4.0/).

1. Introduction

Asphalt binder is the main construction material for flexible pavements, and the worldwide production of asphalt materials is estimated to be more than a billion tons in 2019 [1,2]. End-of-service-life asphalt pavement is milled and collected, producing a large amount of reclaimed asphalt pavement (RAP). RAP application in new pavements can conserve valuable natural resources and reduce greenhouse gas emissions [3,4].

During aging, the elemental ratios and chemical components of the bitumen on the RAP are changed, which results in the deterioration of

* Corresponding author.
E-mail address: P.lin-2@tudelft.nl (P. Lin).

https://doi.org/10.1016/j.matdes.2021.109639
0264-1275/© 2021 The Authors. Published by Elsevier Ltd. This is an open access article under the CC BY license (http://creativecommons.org/licenses/by/4.0/).

the physical and rheological properties of bitumen [5,6]. In the recycling of RAP, the addition of the rejuvenator is an important way to recover the physical and rheological properties of aged binders [7–11]. There are plenty of studies about the effect of rejuvenators on binder rheology. Rejuvenators soften the aged bitumen causing the increase of penetration, ductility, phase angle and colloidal instability index, and decrease of viscosity and complex modulus [3,4,12–18]. Meanwhile, recent investigations have shown a close relationship of microstructure with chemical composition and rheological properties of bitumen [19–23], assisting on understanding the rejuvenation mechanism. However, the rejuvenator's effect on the microstructure of aged bitumen is not well understood yet.

The bitumen microstructure has been intensively investigated with different microscopic methods, such as optical microscopy [24,25], fluorescence microscopy [26–28], transmission electron microscopy [28], atomic force microscopy [29–31] and scanning electron microscopy (SEM) [32–34]. Among these methods, SEM is a promising one to investigate the microstructure morphologies of various binders [35,36]. In the 1980s, the presence of environmental scanning electron microscope (ESEM) improved the observation quality for poorly conductive and viscous oil-bearing specimens, such as bitumen [37–39]. The advantage of the ESEM in the research for oil-bearing materials such as bitumen is that deposition of a conductive metal alloy or carbon coating onto the sample is not required, and the surfaces can be imaged directly. This allows one to conduct in situ studies of the electron-sample and gas-sample interactions as well as fracture studies, where new surfaces are generated during crack propagation [40]. During the examination of bitumen films with ESEM, a modification of the bitumen surface was observed after exposing films to the electron beam for several minutes. The bitumen surface is initially flat but appears as a random network of fibrils after beam exposure [41]. It is envisioned that the electron beam preferentially etches the low molecular weight oils (saturate and aromatic) from bitumen and the remaining portion consists of the higher molecular weight components, usually the asphaltenes and resins. Due to this reason, the fibril structure is highly influenced by the fractions of saturates, aromatics, resins and asphaltenes (SARA) of bitumen, described with colloidal instability index [27].

In the 1990s, a series of investigations reported that "random networks of fibrils" can be observed after several minutes of electron beam exposure with secondary electron signal mode [40–42]. Rozeveld et al. explained this phenomenon as the light molecular component's volatilization due to the localized heating generated by electron beam (200 °C) [41]. The "networks of fibrils" were assumed to be a mix of asphaltenes and resins. The fibril structure was changed by tensile loading, with the strands in the structure aligning themselves parallel to the tensile direction. Stangl et al. investigated the microstructure of bitumen with ESEM and nano-indention tests and found the distance between two adjacent strands in these two different tests was the same, indicating that the fibril structure was not induced by the electron beam [43]. Also, others agreed that the ESEM morphology shows the structure of bitumen rather than the electron beam caused artifact [41,42,44]. Gaskin et al. reported that the electron beam could activate the radiolytic particles and evaporate the light components from the material surface [45].Gaskin also reported the ESEM microstructure of bitumen's SARA fractions and waxes. The maltene fraction exhibited a fibrils structure ubiquitous, which was similar to the structure in bitumen. The maltene might not be free from asphaltene due to the limitation of the extraction technique; at least, the fibril structure also contained the amount of maltene [45]. Recently, Lu characterized the surface of the structured area with time-of-flight secondary ion mass spectrometry (TOF-SIMS), which demonstrated that the aliphatic and aromatic content is higher and lower, respectively, on the surface of the structured area compared with those of unstructured surfaces. With the Principal Component Analysis (PCA), it was speculated that the worm structure might be attributed to the evaporation of volatiles, hardening and local contraction, and possibly to chemical reactions (e.g., breaking of chemical bonds, chain scission and crosslinking). In summary, the formation of the fibril structure and its composition is still not totally clear.

According to other ESEM studies, the bitumen microstructure is also influenced by aging and modification. Rozeveld et al. reported that the addition of styrene-butadiene rubber in bitumen could lead to a significant change of microstructure from a random pattern to textured. Meanwhile, the aging of base bitumen led to a coarser fibril structure and a larger fibril diameter [41]. Mikhailenko et al. reported that with the increased oxidation degree, the fibril structure was denser, more structured and smaller in fibril diameter [46]. The different conclusions in these two studies may be due to the different origin of base bitumens, indicating the influence of aging on the microstructure of bitumens needs further investigation. The addition of styrene-butadiene-styrene increased the fibril diameter and microstructure density [47]. Similar observations were obtained elsewhere [34,43,44,48]. Stangl found that the packing density of microstructure obtained by ESEM correlates well with the change in gel permeation chromatography (GPC) results and viscosity increase [43]. Mikhailenko also reported that the "fibril area" and "formation time" had a good correlation with penetration value and softening point [47]. Overall, the evolution of physical properties corresponds to bitumen microstructure, and the latter can be used as the "fingerprint" of bituminous binders.

Although there are interesting findings in ESEM, limited studies exist on assessing rejuvenators' influence on bitumen. In this study, particular emphasis will be given to providing insights into the rejuvenation mechanism of base and polymer modified bituminous binders, collectively called binders, using ESEM. Particularly, the effect of aging and rejuvenation on the binder microstructure will be evaluated. Moreover, evidence will be provided on rejuvenators' influence on binder microstructure. Finally, a correlation between rheology and ESEM microstructural characteristics will be proposed.

2. Materials and methods

2.1. Binders, rejuvenators and aging protocols

The styrene-butadiene-styrene (SBS) is one of the most widely used thermoplastic polymers for bitumen modification, which can improve the material rutting and thermal cracking resistance [49–51]. A commercial SBS polymer modified bitumen (PMB) was used in this research. The basic rheological and physical properties of PMB are given in Table 1.

Three different products were selected to investigate the effect of rejuvenators on the rheological properties and ESEM microstructural characteristics of aged PMB. The rejuvenator Rej-A is an industrial rejuvenator rich in aromatic compounds. According to the material supplier,

Table 1
Basic rheological and physical properties of PMB binders.

Properties	Measurement	Technical Criterion	Specifications
Original			
Penetration at 25 °C, 100 g, 5 s (0.1-mm)	55	40– 60	ASTM-D5
Softening point (°C)	65.7	>60	ASTM-D36
G*/sinδ @ 70 °C (kPa)	2.408	>1.0 kPa	ASTM-D6373
G*/sinδ @ 76 °C (kPa)	1.419	>1.0 kPa	ASTM-D6373
Glass transition temperature (°C)	−15.4	–	–
RTFOT			
Mass loss (%)	0.22	± 1.0	
G*/sinδ @ 70 °C (kPa)	2.905	>2.2 kPa	ASTM-D6373
G*/sinδ @ 76 °C (kPa)	1.607	>2.2 kPa	ASTM-D6373
Glass transition temperature (°C)	−14.8	–	–
PG Grade	PG 70–22	–	ASTM-D6373

the aromatic type and ratio in Rej-A are designed based on the Hansen solubility parameter, and Rej-A is especially suited for high RAP materials produced at normal asphalt production temperatures (160 °C). Rej-B is a low viscous liquid rejuvenator, rich in saturates and contains selected components for the re-compatibilization of the various phases in oxidized mastic.

Rej-C was fabricated in the lab to rejuvenate the aged PMB. The Rej-C contains saturates, aromatics, SBS copolymer and additives to allow the dispersion of agglomerated asphaltenes. The addition of the saturate component (bio-oil) functions to decrease the viscosity, and the aromatic component (aromatic oil) helps to recover the viscoelastic characteristics of aged PMB. A selected petroleum plasticizer was also added as a stabilizer to improve the miscibility between the polymer and saturated/aromatic oil. Afterward, a plant-extracted oil with cyclic monoterpene was added to disperse the agglomerated asphaltenes. The ratios of different components have been optimized through extensive experiments. The properties and description of all three rejuvenators can be seen in Table 2.

The binders were firstly subjected to short-term aging with Rolling Thin Film Oven Test (RTFOT) (EN12607) at 163 °C for 75 min, and subsequently, long-term aging was conducted in a Pressure Aging Vessel (PAV) (EN14769) at 100 °C for 80 h. The reason for choosing such a long time is that 80 h PAV aging has shown an equivalent aging degree with a porous asphalt surfacing material after ten years of service [52]. Afterward, the rejuvenated bitumen was prepared by blending the aged bitumen and rejuvenator with a mixer under 170 °C for 10 min. The choice of a relatively wide range of rejuvenator dosage (5– 30%) was based on the possibility to observe the microstructure of PMB with ESEM and the rejuvenation propensity of binders. The description of binders can be seen in Table 3.

2.2. Frequency sweep tests

A dynamic shear rheometer (DSR) was applied to characterize the rheology of binders with oscillatory sinusoidal loading. In this study, the DSR tests were conducted in a parallel plate testing configuration with an 8-mm diameter spindle between 0 and 30 °C and a 25-mm diameter spindle between 40 and 80 °C, respectively. Frequency sweep tests from 0.01 to 10 Hz were conducted at 0, 20, 30, 40, 60 and 80 °C with strain amplitude within the linear viscoelastic range. Three replicates per material were tested.

The complex modulus master curves were constructed with the Sigmoidal Model [53,54]. The phase angle master curves were constructed with Kramers-Kronig relations, which was firstly suggested by Booij and Thoone [55,56].

$$log\,|G^*| = \nu + \frac{\alpha}{1 + e^{(\beta+\gamma log\omega)}} \tag{1}$$

$$\delta = 90 \times \frac{dlogG^*}{dlog\omega} = -90 \times \alpha\gamma \frac{e^{(\beta+\gamma log\omega)}}{\left[1 + e^{(\beta+\gamma log\omega)}\right]^2} \tag{2}$$

where ω is the reduced frequency at the reference temperature (rad/s), $|G^*|$ is the complex modulus (Pa), δ is phase angle (degree), ν is the lower asymptote, α is the difference between the values of the upper and lower asymptote, β and γ define the shape between the asymptotes and the location of the inflection point (inflection point obtained from $10^{(\beta/\gamma)}$).

Cavalli proposed an aging index, which was defined to incorporate the changes over a large frequency range by calculating the difference of area between the complex modulus master curves of fresh and aged bitumen over a defined frequency range [57]. Based on this idea, the indices of complex modulus (I_M) and phase angle (I_P) are defined as the ratio of the integral area of master curves of the original binder to that of the rejuvenated one. These two parameters can be applied to characterize the rejuvenation degree. The definition of I_M and I_P are as follows:

$$A_M = \int_{-5}^{4} \log G^*(\omega) d\omega \tag{3}$$

$$A_P = \int_{-5}^{4} \delta(\omega) d\omega \tag{4}$$

$$I_M = \frac{A_{M-Sample}}{A_{M-OB}} \times 100\% \tag{5}$$

$$I_P = \frac{A_{P-sample}}{A_{P-OB}} \times 100\% \tag{6}$$

where A_M is the integral area of complex modulus, $A_{M\text{-}OB}$ and $A_{M\text{-}sample}$ are the A_M of original binder (OB) and rejuvenated binders, A_P is the integral area of phase angle, $A_{P\text{-}OB}$ and $A_{P\text{-}sample}$ are the A_P of original binder (OB) and rejuvenated binder.

The scheme of the definition of complex modulus and phase angle indices can be seen in Fig. 1. When the complex modulus index reaches 100%, the rejuvenated binder will be similar to the original binder according to the complex modulus master curves. These indices provide methods for rejuvenator selection and rejuvenator dosage determination.

2.3. Multiple stress creep recovery tests

The multiple stress creep recovery (MSCR) tests were conducted to evaluate binders' rutting resistance with a 25-mm spindle and 1-mm gap. The binder is subjected to an alternate cycle of 1 s of creep and 9 s of recovery, at 0.1 and 3.2 kPa stress levels, respectively. The MSCR tests were conducted 30 cycles, and the high-temperature performance of binders was evaluated with non-recovery compliance (J_{nr}) and

Table 3
Description of studied binders.

Name	Composition
Base bitumen	Base bitumen before the addition of SBS polymer
OB	Original SBS polymer modified bitumen
RTFOT	SBS polymer modified bitumen after RTFOT aging
4PAV	SBS polymer modified bitumen after RTFOT aging and 80 h of PAV aging
A5,10,15,20,30	4PAV + 5,10,15,20,30% wt Rej-A
B5,10,15,20,30	4PAV + 5,10,15,20,30% wt Rej-B
C5,10,15,20,30	4PAV + 5,10,15,20,30% wt Rej-C

Table 2
Name and properties of rejuvenators.

Rejuvenator	Viscosity at 20 °C (Pa·s)	Density (kg/m^3)	Petroleum/Organic	Main component	Auxiliary components	Polarity
Rej-A	0.817	0.955	Petroleum	Aromatic	None	High
Rej-B	0.115	0.928	Organic	Aliphatic	None	None
Rej-C	0.752	0.943	Mixed	Aromatic & Aliphatic	Polymer & Additves*	Low

Note* The function of additive is to separate the agglomeration of asphaltene.

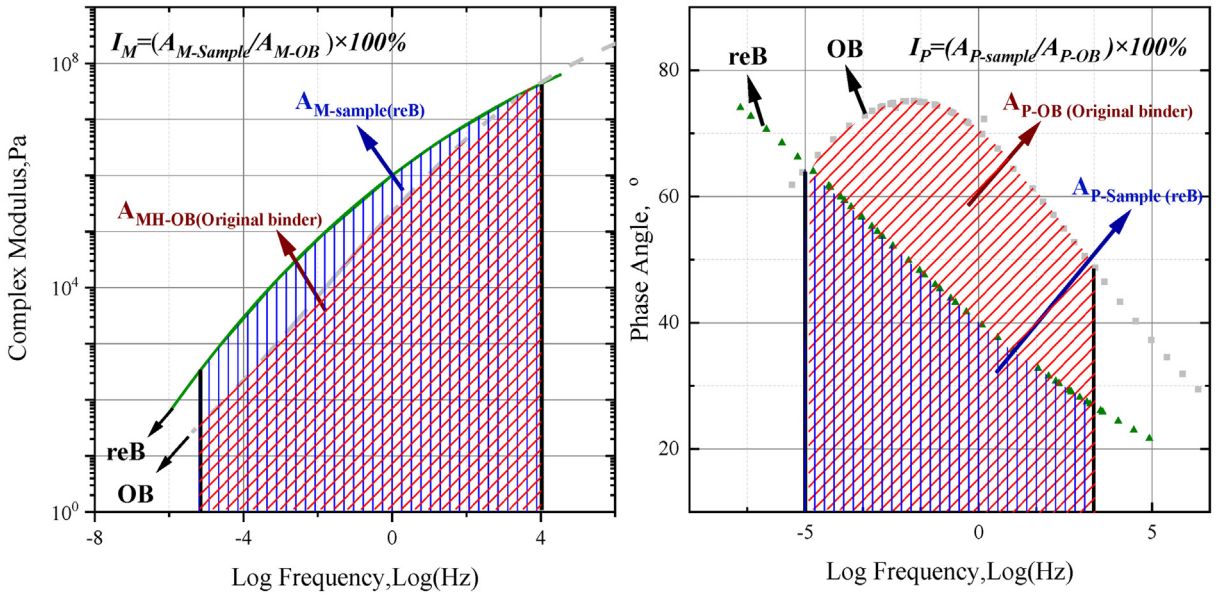

Fig. 1. The scheme of the definition of complex modulus and phase angle indices.

percent recovery (R), whose determination is described in detail in ASTM D7405–08. Three replicates per material were tested.

2.4. Linear amplitude sweep tests

The linear amplitude sweep (LAS) is an accelerated test performed at an intermediate temperature [58,59]. Here, the LAS tests were conducted in DSR with the 8-mm parallel plates to evaluate the fatigue property of binders at 20 °C. According to AASHTO TP 101, the LAS test consists of a non-destructive frequency sweep test and a strain amplitude sweep test. The frequency sweep was conducted with a frequency range from 0.2 to 30 Hz at a strain amplitude of 0.1% to determine the undamaged binder properties. The amplitude sweep is performed with a strain level from 0.1 to 30%. Three replicates per material were tested.

2.5. Environmental scanning Electron microscopy

For the ESEM evaluation of binders, an 8-mm cylindrical holder was prepared. The binders were heated at 150 °C for 30 min. Subsequently, 0.1 g of material was poured on the sample holder with the help of a spatula (Fig. 2(a)). Then, the bitumen-filled holders were placed on a hotplate at 170 for about 60 s for flattening. Before ESEM analyses, all samples were stored in a cooler at 10 °C overnight.

The microstructure assessment of binders was conducted at 25 °C with an ESEM device (Philips XL 30 ESEM). Samples were placed on

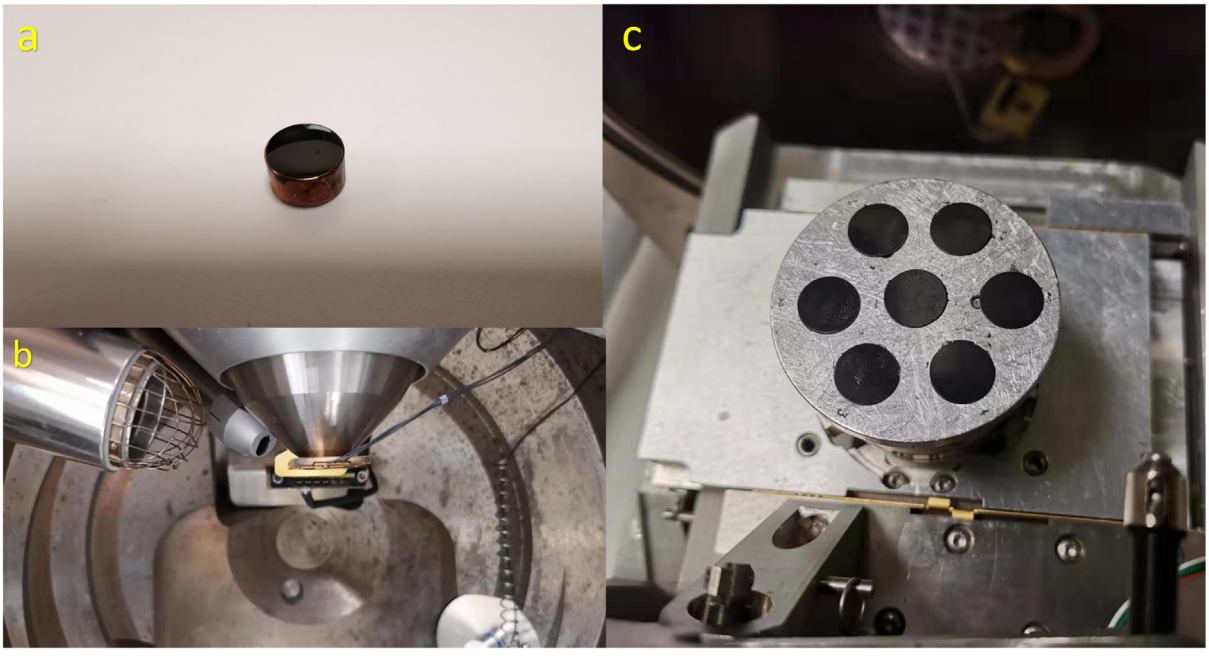

Fig. 2. ESEM device and bitumen sample, (a) bitumen sample, (b) detector and electron gun and (c) ESEM sample stage.

the ESEM sample stage, which is under the ESEM detector and electron gun (Fig. 2**(b,c)**). The microstructure parameters were an acceleration voltage of 20 keV, a spot size of 3.5, a chamber pressure of 1.0 Torr of vapour and three different magnification (250×, 500× and 1000×) in secondary electron (SE) mode [34,48]. The sample was exposed to the electron beam for 20 min for tracking the microstructure changes in binders. ESEM observations for each binder sample were performed three times.

3. Results

3.1. Viscoelastic properties analysis

The viscoelastic properties of the original, aged and rejuvenated binders were characterized with master curves of complex modulus and phase angle. Specifically, as illustrated in Fig. 3(a), the complex modulus of RTFOT aged sample increased slightly at high frequency and increased substantially at low frequency compared with the original sample. The short-term aging mainly led to a modulus increase of PMB at the high frequency (high temperature) range. In terms of phase angle master curves, the original binder exhibited a plateau zone with log frequencies between −3.5 and − 0.5. According to the research of Lu and Airey [60,61], the phase angle plateau zone is caused by the polymer network in PMB. Although the presence of SBS copolymer is more apparent before aging according to the phase angle results in the low-frequency spectrum, the phase angle plateau disappeared after aging, indicating the aging induced degradation of the polymer network [49,62].

As illustrated in Fig. 3**(b-d)**, the addition of the rejuvenator led to a significant decrease of complex modulus and an increase of phase angle both at high and low frequency. The 4PAV aged sample recovered its viscous behavior with the rejuvenator addition. Although all three rejuvenators were able to decrease the complex modulus and increase the phase angle, their rejuvenation effect was different. Rej-B substantially decreased the complex modulus, and Rej-C significantly increased the phase angle at relatively low rejuvenator content.

For further quantitative analysis of the rejuvenator's impact, the I_M and I_P values are calculated and presented in Fig. 4. During aging, the 4PAV aged binder showed a 28% increase in I_M and 28% increase in I_P comparing to the original binder. When rejuvenator content is low, there is no significant difference between rejuvenators. However, when rejuvenator content is higher than 15%, Rej-B was more effective

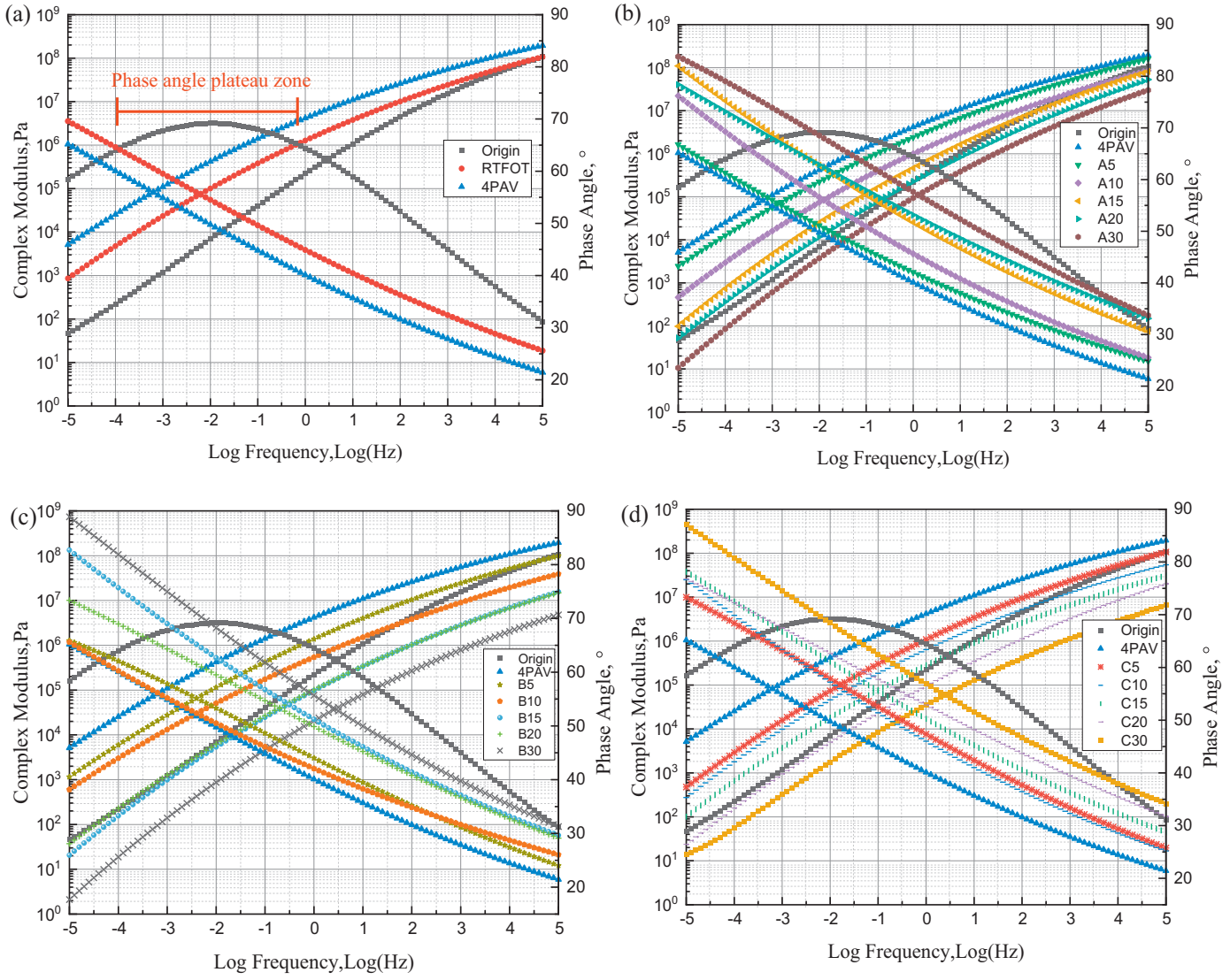

Fig. 3. Complex modulus and phase angle master curve of origin, aged and rejuvenated PMB binders at a reference temperature of 30 °C, (a) origin and aged PMB, (b) rejuvenated bitumen with Rej-A; (c) rejuvenated bitumen with Rej—B; (d) rejuvenated bitumen with Rej—C.

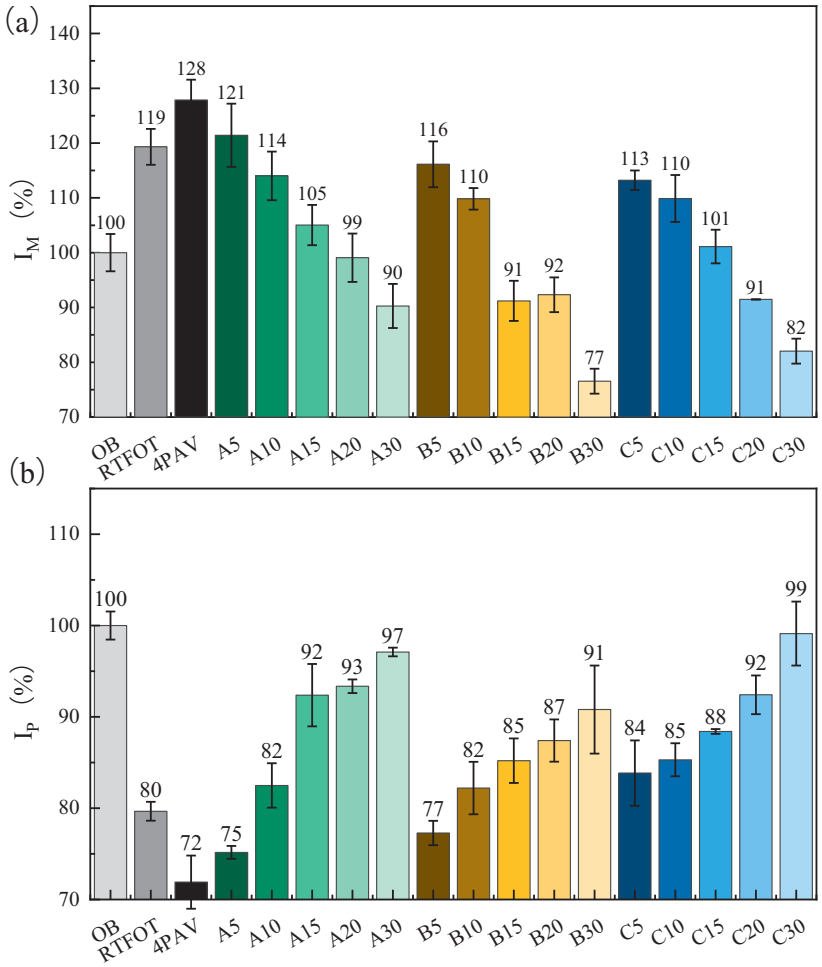

Fig. 4. Complex modulus index and phase angle index of origin, aged and rejuvenated PMB binders, (a) complex modulus index; (b) phase angle index.

in decreasing complex modulus compared with Rej-A, and Rej-C and Rej-A are more efficient in increasing phase angle compared with Rej—B.

3.2. MSCR analysis

To evaluate the impact of rejuvenator on rutting resistance, the MSCR tests were conducted at 70 °C. The average non-recoverable creep compliance ($J_{nr3.2}$) and average percent recovery at 70 °C were demonstrated in Fig. 5. The RTFOT aged binder has shown slightly lower $R_{3.2}$ and $J_{nr3.2}$ compared with the original binder. However, after 4PAV aging, the $R_{3.2}$ increased, and the $J_{nr3.2}$ decreased dramatically. According to previous studies [52,62], the degradation of the polymer network plays a dominant role in short-term aging at a relatively high temperature (163 °C), causing a decrease in elastic recovery ability. After 80 h of PAV aging, the severe oxidation of the bitumen phase plays the dominant role, which increases the stiffness and elasticity of PMB.

With the increase of rejuvenator content, $R_{3.2}$ decreased, and $J_{nr3.2}$ increased extensively, indicating loss of elastic recovery ability and decrease of rutting resistance. Among these rejuvenators, the rejuvenated bitumen with Rej-C showed higher $R_{3.2}$, especially when the rejuvenator content was less than 15%. It might be caused by the addition of SBS copolymer in Rej—C, which could supplement the degraded polymer. However, the rejuvenated binder with Rej-A has shown relatively lower $J_{nr3.2}$, indicating that this rejuvenator probably had a less adverse impact on rutting resistance. Most rejuvenated binders satisfied the criteria of maximum $J_{nr3.2}$ as given by AASHTO MP19 for heavy traffic conditions, except the rejuvenated bitumen with 30% of Rej—B. Although the addition of the rejuvenator decreases elastic recovery and rutting resistance, it is restoring the original behavior of the bitumen, which tends to be stiffer after aging.

3.3. LAS analysis

The LAS tests were conducted to evaluate the fatigue life of all binders. The fatigue life at 2.5% ($N_{f2.5}$) and 5% (N_{f5}) strain levels are illustrated in Fig. 6. After aging, the $N_{f5\%}$ of PMB decreased from 340 cycles (original binder) to 268 cycles (RTOFT aged binder), and finally to 143 cycles (4PAV aged binder). The addition of the rejuvenator was effective in recovering the fatigue property of the aged PMB binder, especially when the rejuvenator dosage was more than 10%, the fatigue life of the rejuvenated binder was higher than that of the original binder. Rej-A showed relatively less improvement in $N_{f5\%}$ in these three rejuvenators, indicating the aromatic component was less efficient in improving fatigue properties. In contrast, Rej-C was more efficient in improving the fatigue properties of the aged binder, probably due to the positive effect of the addition of SBS copolymer. The evolution of $N_{f2.5\%}$ for rejuvenated bitumen was consistent with the evolution of $N_{f5\%}$.

3.4. ESEM analysis

3.4.1. Microstructure morphology

ESEM is a robust imaging technique to characterize the microstructure morphology of various materials, including wet, oily and non-conductive

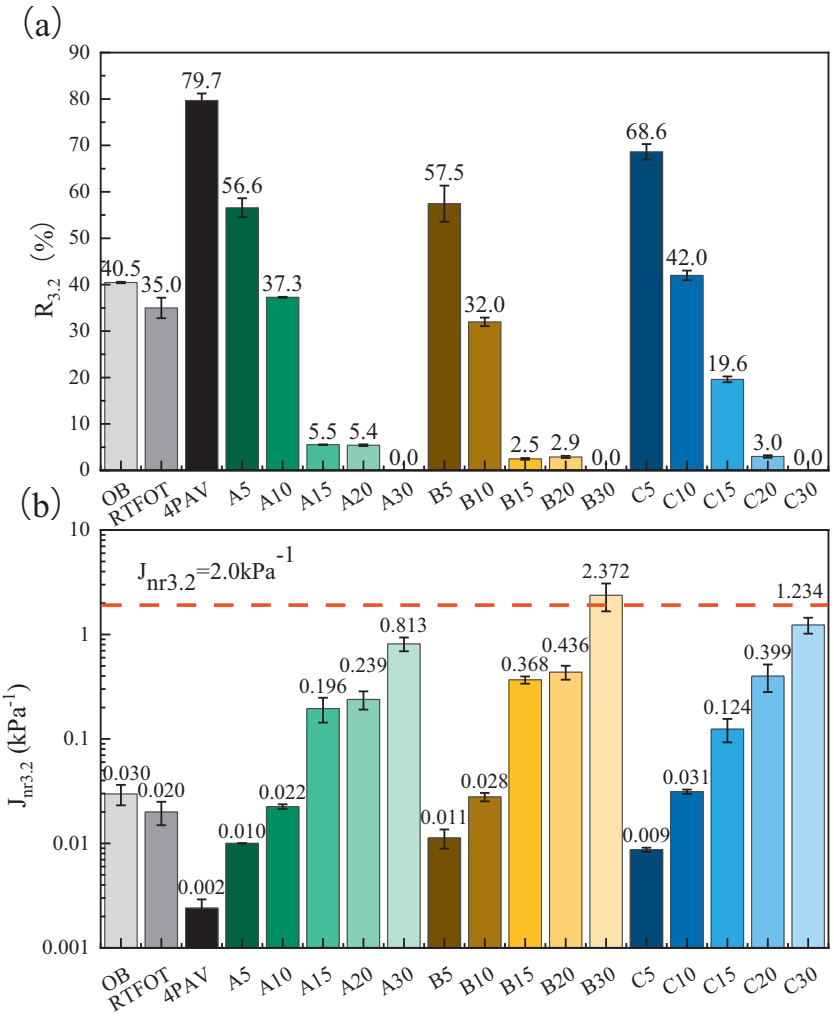

Fig. 5. MSCR results of origin, aged and rejuvenated PMB binders, (a) percent recovery at 3.2 kPa, (b) non-recoverable compliance at 3.2 kPa.

substances in their original state [34]. Firstly, three types of rejuvenators were investigated with this technique, and the ESEM images are illustrated in Fig. 7. Initially, there was a "needle" structure on the surface of Rej—B, which is similar to the ESEM image of base bitumen incorporating a bee-like structure [34,45]. It was speculated that the bee structures were caused by waxes, which may form crystal networks attributed to diffusion or spontaneous alignment [63]. In this research, Rej-B may contain paraffin waxes associated with the "needle" like structures. However, after 3 min of illumination, these structures totally disappeared (Fig. 7 **(b)**). Also, no changes were observed when the Rej-B was subjected to 20 min of illumination. Similarly, the Rej-A and Rej-C were subjected to 20 min of illumination, and no obvious structure was observed (Fig. 7 **(c)** and **(d)**).

Here, after a period of illumination, the binders were investigated with ESEM and a fibril structure was observed, as shown in Fig. 8. The fibril structures of binders were quite similar as demonstrated in **Fig. 8(a)** and **(b)**, respectively. The fibril structure of PMBwas slightly denser (covers more area of the surface) of larger strand diameter than of base bitumen. The RTFOT aging induced a significant evolution of fibril structure in binder, in which the strand diameter became smaller, and the surface became rougher. After 4PAV aging, the fibril structure was not observed even after 20 min of illumination, and a few bubble-like spots appeared (Fig. 8(d)). It is because the electron beam preferentially etches the low molecular weight oils from bitumen and the remaining portion consists of the higher molecular weight components, usually the asphaltenes and resins [43,64]. During long-term aging, the content of the evaporable component decreased, and the fibril structure cannot be seen anymore. The formation mechanism of the bubble-like spot needs further investigation.

To reveal the influence of rejuvenator on the microstructure of the aged binder, sixteen different rejuvenated binders were investigated in ESEM, and the results are shown in Fig. 9**.** For the rejuvenated bitumen with Rej-A, the ESEM images were flat and featureless with less than 15% of rejuvenator, just like the 4PAV aged bitumen. The fibril structure appeared again when the content of Rej-A was more than 20%. The fibril structure of A20 (aged PMB binder rejuvenated with 20% of Rej-A) and A30 were rougher and more perpendicular structurally than of the original microstructure. 15% of Rej-B was needed in bitumen for the re-appearance of the fibril structure. The fibril structure of B15 appears to be "random", which is similar to the structure of the original PMB. With the increase of Rej-B content, the fibril structure became sparse and perpendicular. The addition of 10% of Rej-C could enable the fibril structure to reappear after the electron beam illumination. This phenomenon agrees with the results of I_P and I_M in which the addition of 10% Rej-C already had a significant rejuvenation effect. This may be due to the role of additives in Rej-C that dissolve and separate the asphaltene agglomeration. With the increase of Rej-C

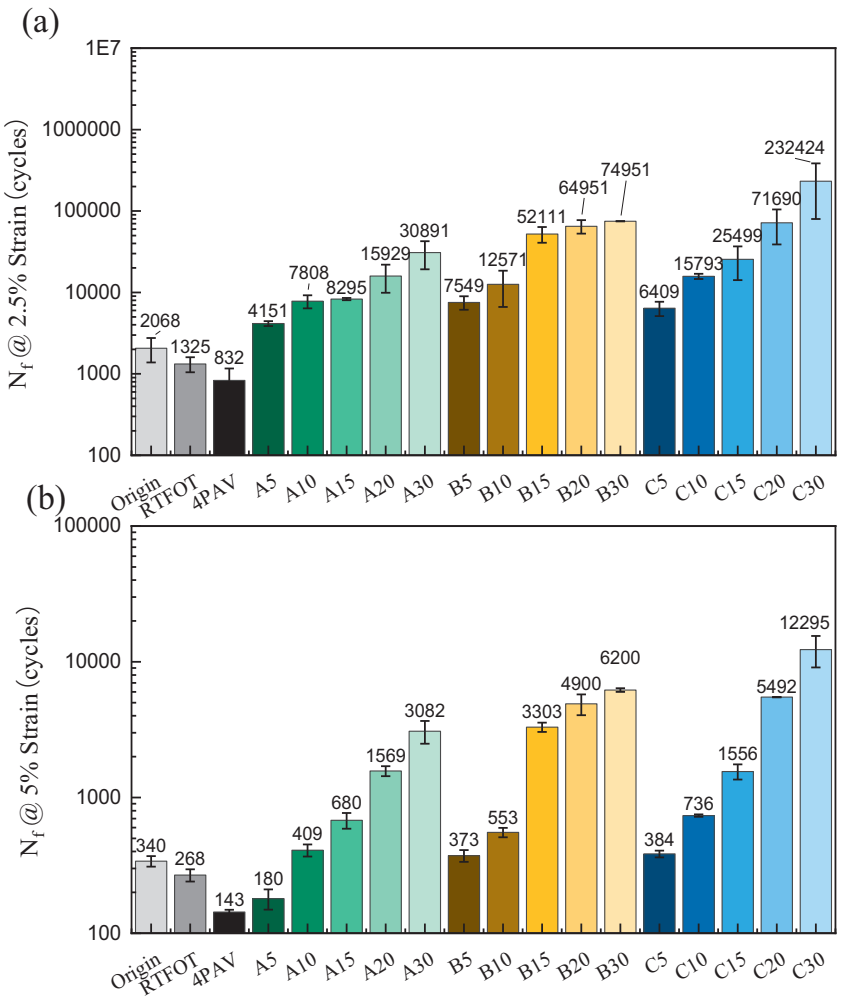

Fig. 6. LAS results of origin, aged and rejuvenated PMB binders, (a) fatigue life at 2.5% strain level; (b) fatigue life at 5% strain level.

content, the strand diameter appeared to be larger, and the fibril structure became smoother, sparser and more perpendicular.

3.4.2. Fibril formation time

The ESEM image of bitumen is flat and featureless at the beginning. With the increase of the illumination time, the fibril structure appeared. From the literature, the time period to obtain a stable ESEM image is called formation time [47]. The formation time essentially reflects the possibility and rate of volatilization of the light molecular component on the surface of bitumen, and it correlates well with aging degree [34,48,65]. Hence, formation time has the potential to be a parameter for characterizing the degree of aging and rejuvenation of bitumen. The evolution of ESEM images of rejuvenated PMB was demonstrated in Fig. 10. All the samples were featureless at the beginning, and after 1 min of illumination of the electron beam, B20 showed a blur fibril structure. A20 and C20 dimly revealed a little of the outline. When the illumination time was 3 min, the fibril structure was revealed and remained unchanged afterward.

To quantitatively analyze the formation time, the evolution of the ESEM image was recorded as a video to precisely extract the formation time data. From previous literature, the fibril structure can only be revealed when the electron beam etches the evaporable component in the surface layer [41,60]. According to previous research [34], it may be because the lighter components of the 4PAV aged binder were not enough to form the fibril structure. The addition of rejuvenators supplements the saturate and aromatic components, allowing the fibril structure formation also decreasing the formation time. Thus, the formation time can be used as a parameter to characterize the degree of rejuvenation. The formation time will not be recorded if the fibril structure did not appear even after 20 min of illumination. As shown in Fig. 11, the formation time increased after RTFOT aging, which is coherent with Mikhailenko's finding [65]. At the same time, the addition of rejuvenators can significantly decrease the formation time. Among the three rejuvenators, Rej-B was most effective in decreasing the formation time. 30% of Rej-B reduced the formation time to 42 s, which is much lower than that of the original sample. However, the formation time of A30 was 138 s, more than three times that of B30. The efficiency of Rej-C in decreasing formation time is between Rej-A and Rej—B.

3.4.3. ESEM image quantification

For further quantitative analysis of the ESEM images, a process was conducted to extract the microscopic parameters of fibril structure, which is based on Stangl and Mikhailenko's work [43,48]. Firstly, the boundary line around the fibril was drawn manually with Image Pro Plus to separate the image into a fibril structure area and a non-fibril structure area. The grey value of the non-fibril area was substitute with black (0) or white (255) for differentiation (Fig. 12 **(a)**). Then, the total fibril area and percent of fibril area coverage were calculated. Secondly, the midline for each fibril was drawn and the total length of the fibril was calculated in the image (Fig. 12 **(b)**). Thirdly, the diameter

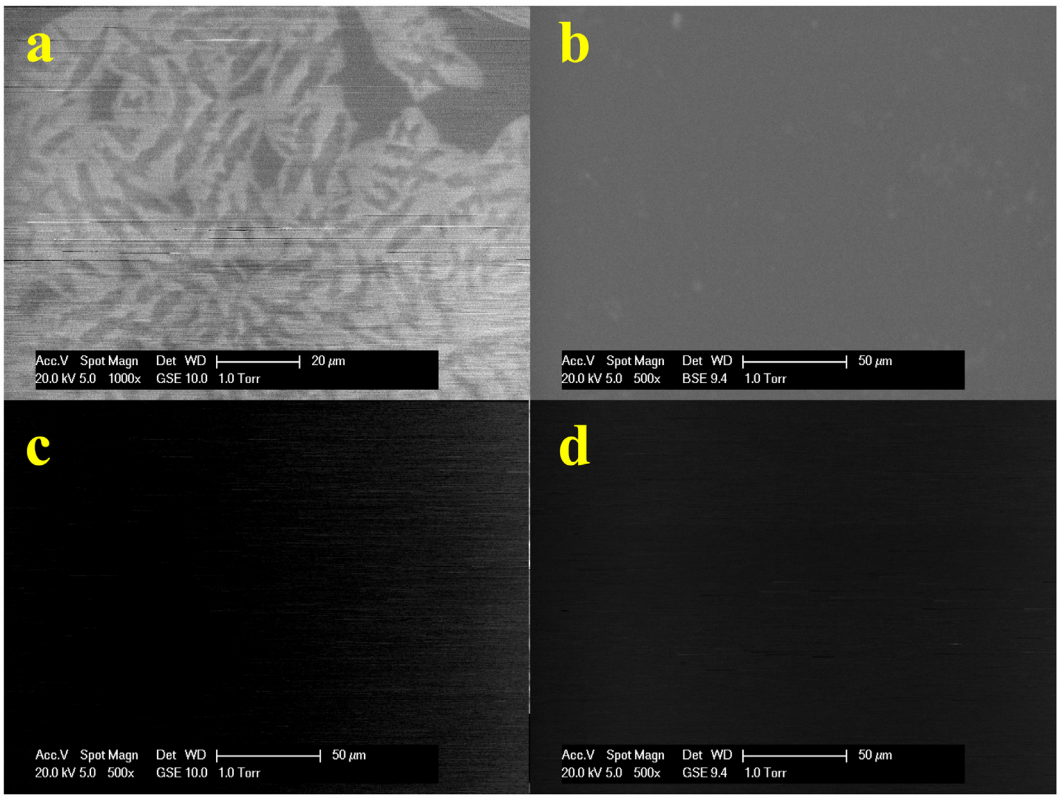

Fig. 7. Microstructure visualized by ESEM for rejuvenators, (a) Rej-B without illumination, (b) Rej-B after 3 min of illumination, (c) Rej-A and (d) Rej-C (20 kV, SE, 500×, 1000×).

of each fibril was drawn, and the average of fibril diameter was calculated (Fig. 12 **(c)**). Finally, the distance between two adjacent fibrils midline was extracted, and the average distance between adjacent fibrils was calculated.

Assuming that the bitumen microstructure's morphology is isotropic, the 2-D ESEM image can be extracted in the 3rd direction. In this way, a simple frame model can be established (Fig. 13). Based on these extracted parameters, the package density (volume fraction) can be calculated:

$$A_s = \frac{d^2 \times \pi}{4} \tag{7}$$

$$V_s = 3 \times \left[\frac{A_s}{4} \times \left(\frac{a}{2} - \frac{\sqrt{A_s}}{2}\right) + \left(\frac{\sqrt{A_s}}{2}\right)^3\right] \tag{8}$$

$$f_s = \frac{V_s}{(a/2)^3} \times 100\% \tag{9}$$

where the A_s is the cross-sectional area of a fibril; d is the average diameter of fibril structure; V_s is the volume occupied by fibril structure; a is the average space between two adjacent fibrils, f_s the volume density of the fibril structure.

The ESEM images were segmented and examples can be seen in Fig. 14. The parameter extraction and quantitative analysis process were conducted afterward, and the results were illustrated in Table 4.

As illustrated in Table 4, the fibril area of the PMB binder increased after RTFOT aging, which agreed with the results of Mikhailenko [48,65]. Only the addition of more than 20% of Rej-B and Rej-C was able to reduce the fibril area significantly. In other cases, the addition of the rejuvenator had no significant effect on the fibril area but mainly changed the diameter of the fibril structure. The average diameter of fibril structure (a) and the average distance between adjacent fibrils (d) increased with a higher content of rejuvenator, especially for B30 and C30. The A_s and V_s parameters exhibited similar patterns of change with the addition of a rejuvenator. However, the variation of f_s is quite complex, and there is no obvious pattern.

4. Principal component and correlation analysis

4.1. Principal component analysis (PCA)

It is not possible to directly formulate a link between ESEM-induced microstructural changes and the rheology of binders. The PCA was applied to explore the rheological and microstructure data, reduce the dimensionality of the data and propose a link between various variables. The PCA analysis can enable the identification of systematic variations in the data by combining parameters (i.e., rheological and microstructure parameters) that vary in the same (or opposite) manner between different binders and turn these combinations into a new set of parameters (principal component, PC). Therefore, the PC1 accounts for the maximum amount of variation in the data and PC2 accounts for the maximum of the remaining variation. Usually, the first two PCs are enough to explain the majority of the data variance (>70%) and generate two graphic outputs called loading plot and score plot [66,67].

In this research, a set of data containing 10 samples and 15 parameters is analyzed with PCA. The detailed data can be seen in Table 5. According to the results of PCA, the first two principal components PC1 (69.3%) and PC2 (14.4%) can explain 83.7% of the total variance.

The loading plot in Fig. 15(a) provides information about the relation between original variables (i.e., rheology and ESEM structure) and principals components (PC1 and PC2). The loading plot mainly reflects the

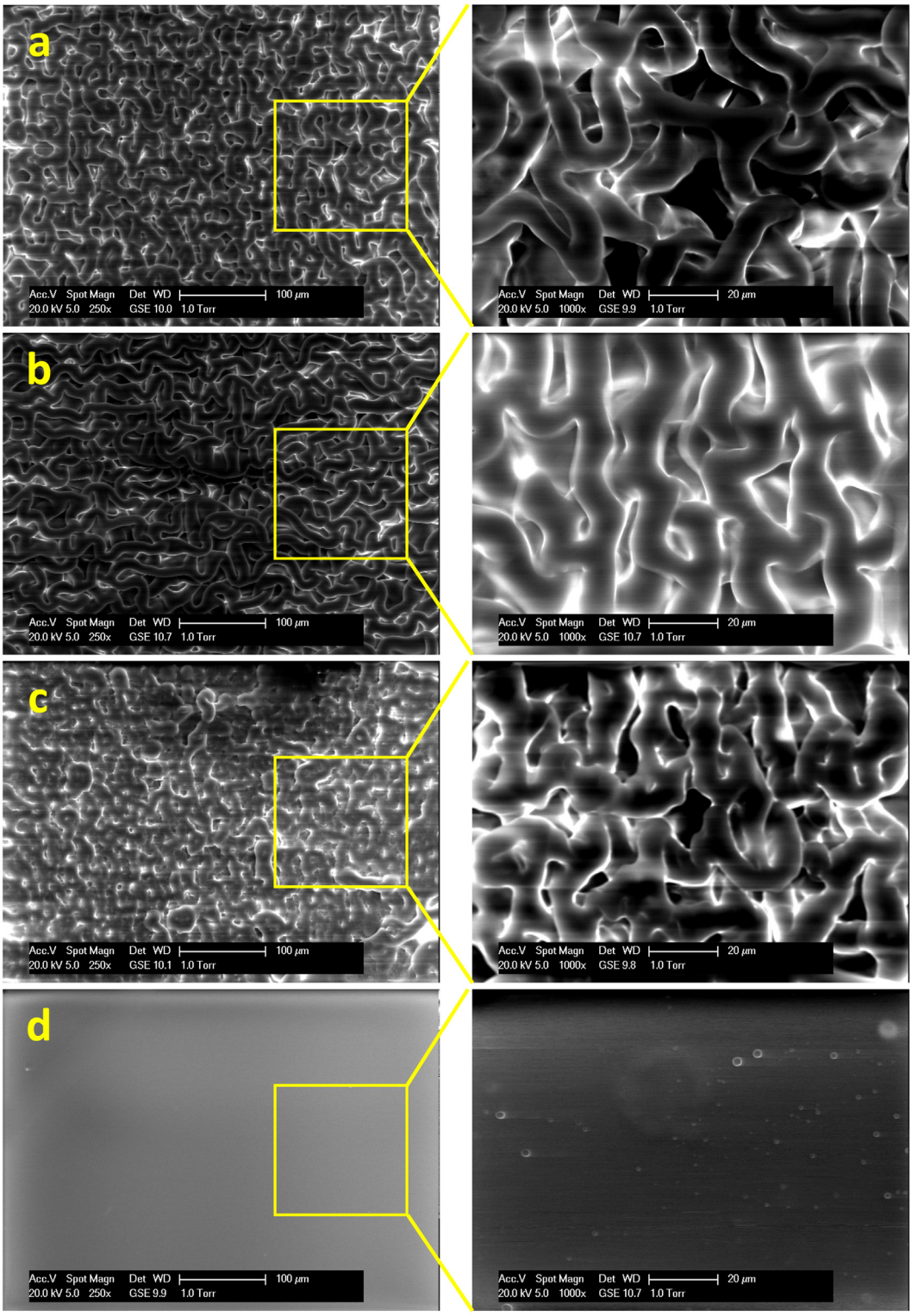

Fig. 8. Microstructures of binders visualized by ESEM, (a) base bitumen, and (b) original, and (c) RTFOT aged, (d) 4PAV aged SBS modified bitumen (20 kV, GSE, 250×, 1000×).

correlation matrix of different parameters. When the vector of the two parameters are close in direction, then it indicates that they are likely to have a positive correlation relationship [66].

From Fig. 15(a), $J_{nr3.2}$ and PC1 are almost in the same direction, which indicates that these two variables have a positive correlation relationship. As $J_{nr3.2}$ indicates the non-recoverable compliance, it can be deduced that the positive direction of PC1 indicates a binder of low stiffness. In terms of ESEM structural parameters, fibril structure diameter (d) and distance between adjacent fibrils (a) are negatively correlated with the stiffness of the binder. Meanwhile, the formation time

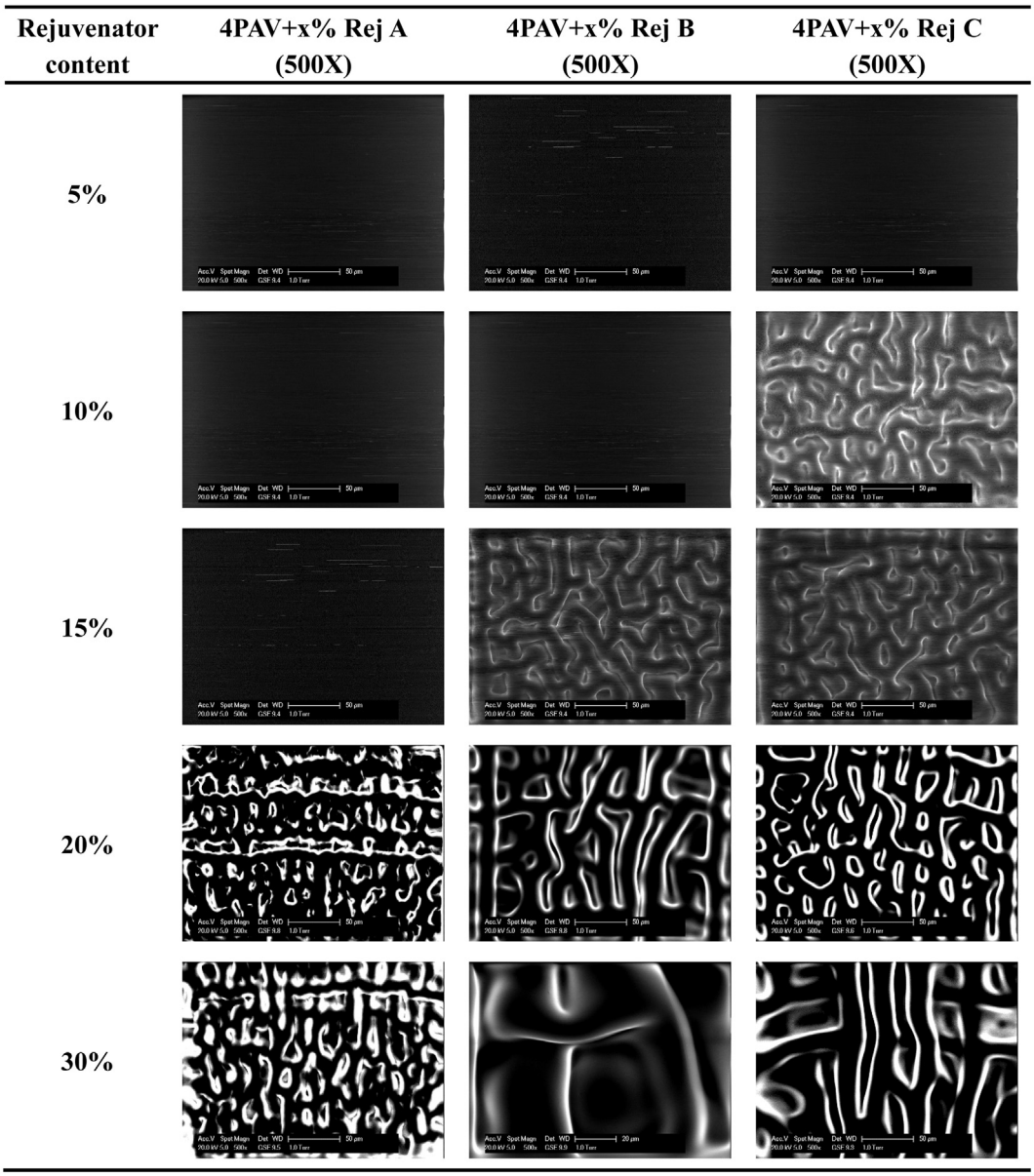

Fig. 9. Microstructures visualized by ESEM for 4PAV aged PMB binder with different types and content of rejuvenator (Illumination time:20 min, Magnification: 500×).

and fibril length are positively correlated with the stiffness of the binder. PC2 is relatively consistent with the phase angle index (I_P), which indicates that PC2 can be used to describe the viscoelastic property of binders. However, no ESEM microstructure parameter was found to correlate well with the PC2. The percent recovery ($R_{3.2}$), fatigue life ($N_{f2.5}$ and N_{f5}) and complex modulus index (I_M) were influenced by PC1 and PC2, indicating that they were influenced by the binder rheology. Correspondingly, fibril area coverage, fibril structure volume (V_s), and fibril package density (fs) are related to the stiffness and the viscoelastic property of the binder.

The results of PCA were also illustrated in a score plot (Fig. 15 (b)), in which each data point corresponds to a binder, and the location of data points reflects the property difference on the scale of PC1 and PC2. According to the loading plot, the negative PC1 indicates binders of high stiffness(low Jnr3.2 and high G*), while the positive PC2 indicates binders of high elasticity (low δ and high R3.2). As illustrated in Fig. 15 (b), the stiffness and elasticity of the binder increased during RTFOT aging. The addition of Rej-A mainly recovered viscous property but did not have a significant effect on stiffness reduction. Considering the main component of Rej-A is an aromatic fraction, it indicates that the main role of the aromatics fraction in rejuvenator is to recover viscous property rather than a decrease of stiffness. In contrast, Rej-B is composed of a saturate fraction without any aromatics. The addition of Rej-B dramatically decreased the stiffness and increase the elasticity of the binder, suggesting the saturate fraction mainly played a role in reducing the stiffness. The hybrid rejuvenator Rej-C was a mix of aromatics, saturates, polymer and additives, which separates asphaltenes' agglomeration. With the increase of Rej-C content, rejuvenated bitumen's stiffness decreased, and viscous property increased. In summary, the composition of the rejuvenator has a decisive influence on the rejuvenation mechanism and the rejuvenation effect it achieves.

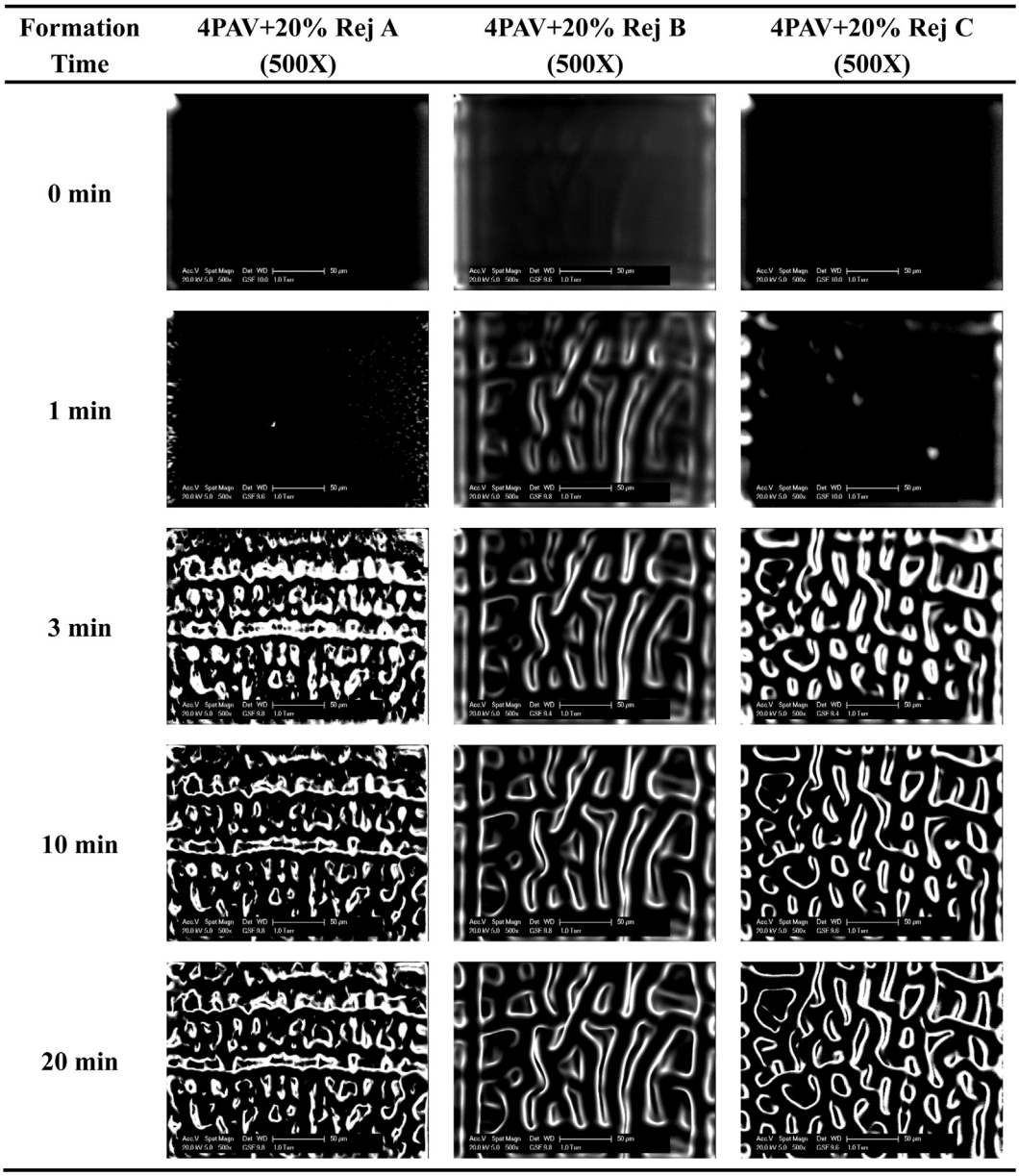

Fig. 10. Evolution of microstructures visualized by ESEM for rejuvenated bitumen at different illumination times.

4.2. Correlations between ESEM structural parameters and rheological parameters

If the vectors of two parameters are close in the same (opposite) direction, the PCA loading plot indicates a positive (negative) correlation between these two parameters. Based on PCA results in Fig. 15, regression analysis was conducted for the ESEM structure parameters and rheological properties. The regression results and fitted equation are presented in Fig. 16.

From Fig. 16 **(a)**, fibril structure diameter (d) and distance between adjacent fibril (a) exhibited a very significant linear relationship ($R^2 = 0.93$), indicating that the increase of parameter ***a*** often accompanied an increase in parameter ***d***. This finding is coherent with the conclusion in the literature [47,65]. The difference is that their investigation showed a simultaneous decrease of ***a*** and ***d*** due to aging, while this study exhibited an increase of ***a*** and ***d*** due to rejuvenation. Meanwhile, there was a negative linear correlation between formation time and a (Fig. 16 **(b)**), indicating the addition of rejuvenator made the fibril structure sparse and easy to emerge under the electron beam's illumination. Fig. 16 **(c)** illustrated an exponential decrease in total fibril length with an increase in ***d***, and **Fig16 (d)** demonstrated that **Vs** decreased linearly with the increase of percent of fibril area coverage. The remarkable correlation of ESEM structural parameters indicated that the morphology of fibril structure always obeyed a certain distribution pattern, regardless of how it changed with aging and rejuvenation.

The ESEM structural parameters are also well correlated with rheological parameters. As illustrated in Fig. 16 **(e)** and **(f)**, with the increase of a, $J_{nr3.2}$ increased linearly while the I_M decreased exponentially. It implies that a sparse fibril structure suggests a binder of low stiffness. From the PCA loading plot, fibril structure density (f_s) may have a correlation with percent recovery ($R_{3.2}$) and fatigue life (N_{f5}). However, Fig. 16 **(g)** and **(h)**, illustrated that

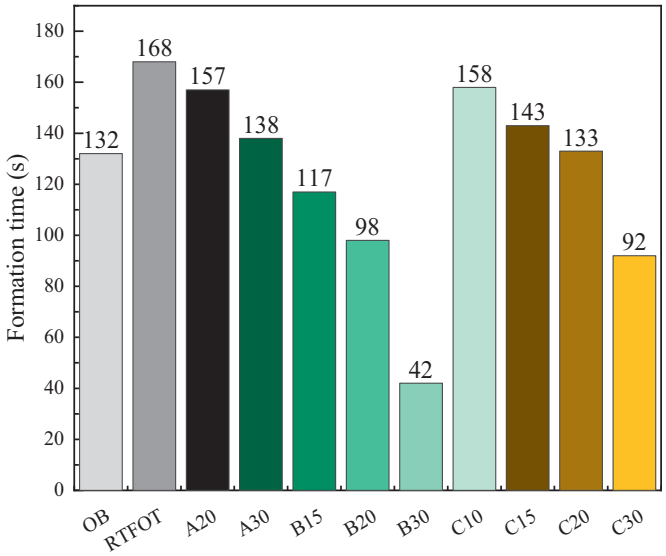

Fig. 11. ESEM fibril microstructure formation time.

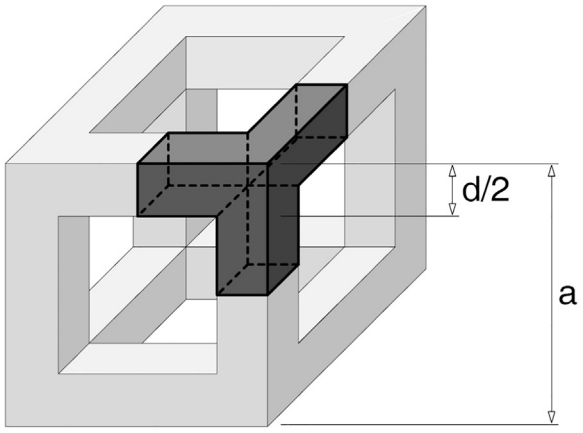

Fig. 13. Model for quantification of parameters of fibril structure of the bitumen microstructure (d: average fibril diameter; a: average space between two adjacent fibrils) [43].

there is no correlation between f_s and $R_{3.2}$, and there was a weak exponential correlation between f_s and N_{f5}. It may be the fact that $R_{3.2}$ and N_{f5} are influenced by both stiffness and phase angle of the binder.

5. Discussion

In this paper, the aging and rejuvenation process of binders manifests how chemical composition affects their rheological properties and microstructure. In agreement with previous studies [68–70], it is believed that the change of chemical composition results in the change of colloidal structure, which is subsequently reflected in the change in binder microstructure and rheological properties. The colloidal structure can act as a bridge to connect the chemical composition, microstructure and rheological properties. Evidence to support this statement is as follows.

Firstly, both aging and rejuvenation correspond to microstructural changes in binders as observed in ESEM. In earlier studies [53,62], the increase of asphaltenes in SBS modified bitumen due to aging was reflected by the FTIR and GPC results, which led to an increase of

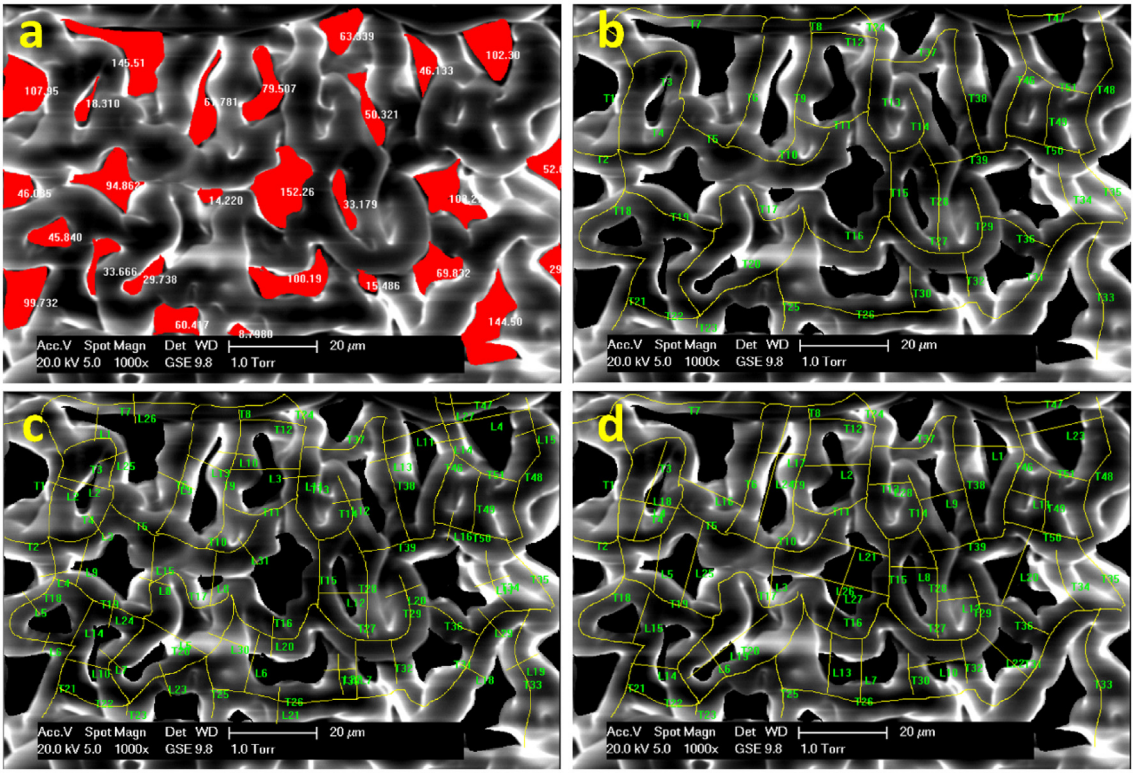

Fig. 12. The process to extract microscopic parameters from ESEM images, (a) definition and calculation of fibril structure area; (b) definition of the midline of fibril structure and calculation of the total length of fibril structure; (c) calculation of the fibril structure diameter, (d) calculation of the distance between adjacent fibrils.

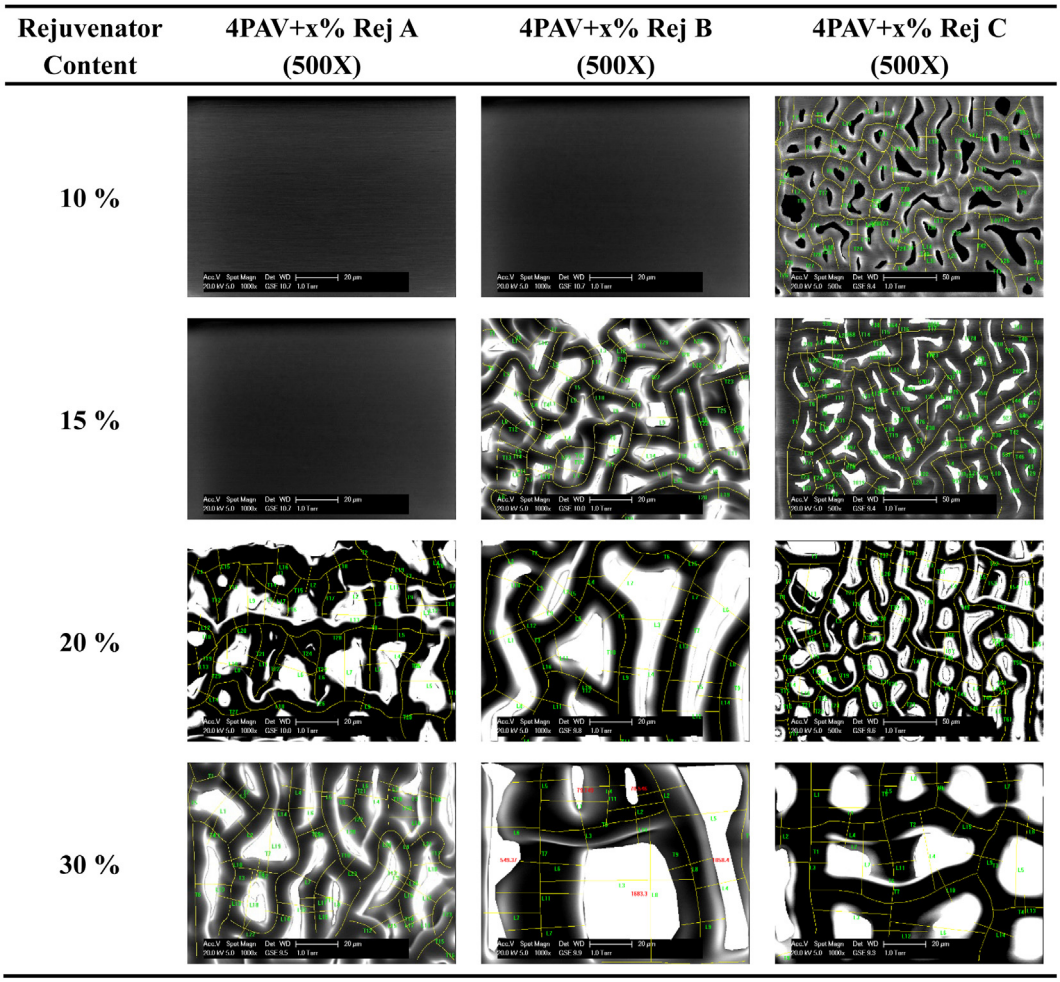

Fig. 14. Examples of sample segmentation for aged PMB binder with rejuvenators.

stiffness and elasticity or an increase of I_M and decrease of I_P and $J_{nr3.2}$. Meanwhile, this phenomenon was also observed in ESEM measurements, as the fibril structure turned to be denser and harder to be revealed (an increase of *formation time*, *area/volume coverage* and decrease of *a* and *d*). Furthermore, the addition of the rejuvenator increased the content of maltenes in bitumen, decreased the stiffness and elasticity. The ESEM microstructure is also turned looser and easier to be revealed. For example, when Rej-B's addition increases from 20 to 30%, the I_M decreased from 92.3 to 76.5%. Simultaneously, the average distance between fibrils increased, the fibril structure turned to be sparse, and the area coverage decreased from 83.8 to 70.0%.

Secondly, the relationship between rheological properties and ESEM microstructure parameters was revealed with the PCA-loading plot. The influence of chemical compositional change due to the addition of rejuvenators was also illustrated in the PCA-score plot. All the rheological and ESEM structural parameters were explained into two principal components (PC1 and PC2). PC1 explained the stiffness of bitumen, and the parameters with vector direction close to PC1 could also be

Table 4
Parameters of ESEM fibril microstructure.

Binder	Fibril area	Area coverage	Total fibril length	d (μm)		a (μm)		As	Vs	fs
	(μm^2)	%	(μm)	Mean	Std. Dev.	Mean	Std. Dev.	(μm^2)	(μm^3)	%
OB	10,022	89.1	1169.1	9.7	3.0	14.5	4.4	73.6	243.3	63.4
RTFOT	10,376	92.3	1197.4	7.9	1.1	13.0	2.9	48.9	152.4	55.8
A20	9850	87.6	1020.9	10.6	1.6	18.4	6.9	88.8	404.9	51.6
A30	10,122	90.0	852.2	12.6	1.7	20.0	3.9	124.6	584.7	58.9
B15	9915	88.2	1302.3	12.3	1.7	18.6	2.0	119.2	507.0	62.8
B20	9418	83.8	585.7	17.3	2.8	24.2	4.0	236.0	1232.8	69.8
B30	7872	70.0	387.0	26.1	8.3	48.9	17.6	535.7	6719.7	46.0
C10	9843	87.6	1500.2	7.9	2.1	11.2	1.2	49.5	120.0	69.1
C15	9945	88.5	1423.0	9.1	1.7	13.0	2.0	65.5	187.3	67.9
C20	10,046	89.4	1368.0	10.3	1.3	15.9	2.7	83.8	306.9	61.4
C30	9278	82.5	539.6	16.9	3.9	35.3	5.2	225.3	2135.0	38.9

Table 5
Data sets for principal component analysis.

Sample	Rheological Parameters						ESEM microstructure parameters						
	Nf2.5	Nf5	IM	IP	R3.2	Jnr3.2	Formation time	Fibril Area	Area Coverage	Total Fibril Length	d	a	As	Vs	fs
	cycle	cycle	%	%	%	kPa-1	s	(μm2)	%	(μm)	(μm)	(μm)	(μm2)	(μm3)	%
Origin	2067.7	340.0	100.0	100.0	40.5	0.03	132	1220.0	89.1	1169.1	9.7	14.5	73.6	243.3	63.4
RTFOT	1325.0	268.0	119.3	79.7	35.0	0.02	168	1809.0	83.9	1197.4	7.9	13.0	48.9	152.4	55.8
A20	15,929.2	1568.9	99.1	93.4	5.4	0.24	157	1392.0	87.6	1020.9	10.6	18.4	88.8	404.9	51.6
A30	30,890.8	3081.9	90.3	97.1	0.0	0.81	138	1120.0	90.0	852.2	12.6	20.0	124.6	584.7	58.9
B15	52,110.7	3303.2	91.2	85.2	2.5	0.37	117	1326.6	88.2	1302.3	12.3	18.6	119.2	507.0	62.8
B20	64,950.8	4900.2	92.3	87.4	2.9	0.44	98	1824.0	83.8	585.7	17.3	24.2	236.0	1232.8	69.8
B30	74,950.8	6200.2	76.5	90.8	0.0	2.37	42	3370.0	70.0	387.0	26.1	48.9	535.7	6719.7	46.0
C10	15,793.3	735.7	109.9	85.3	42.0	0.03	158	1399.0	87.6	1500.2	7.9	11.2	49.5	120.0	69.1
C15	25,498.6	1555.8	101.1	88.4	19.6	0.12	143	1297.5	88.5	1423.0	9.1	13.0	65.5	187.3	67.9
C20	71,690.3	5492.0	91.5	92.4	3.0	0.40	133	1196.0	89.4	1368.0	10.3	15.9	83.8	306.9	61.4
C30	232,424.1	12,295.3	82.0	99.1	0.0	1.23	92	1964.0	82.5	539.6	16.9	35.3	225.3	2135.0	38.9

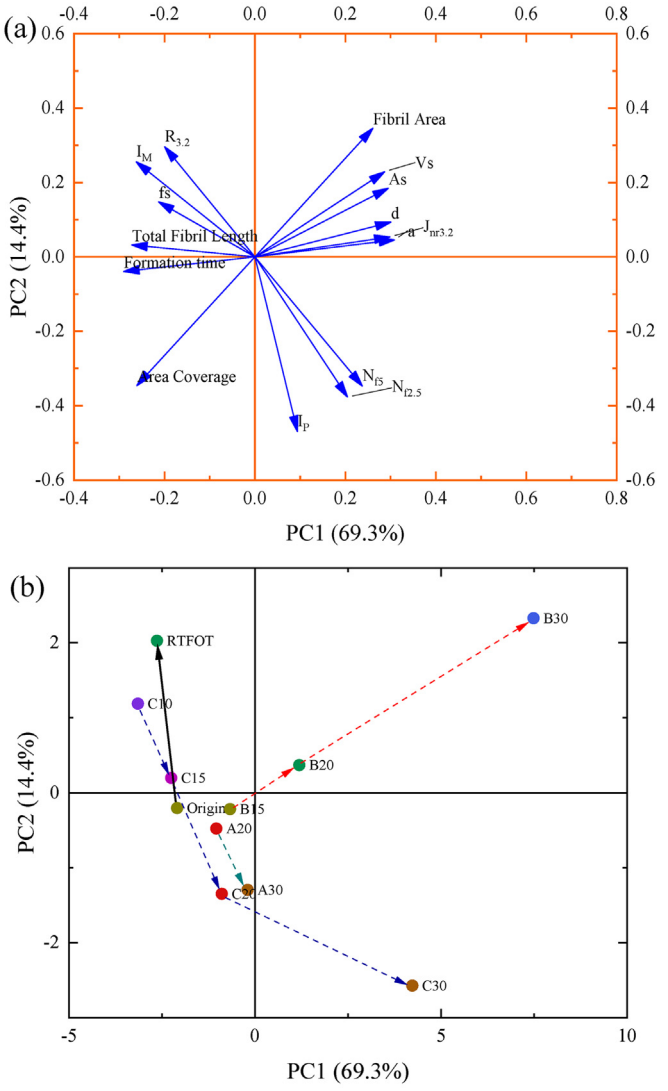

Fig. 15. PCA: (a) loading and (b) score plot.

used to characterize bitumen's stiffness. In this way, the larger *total fibril length* and *formation time*, the smaller *a* and *d*, indicating a binder of higher stiffness. PC2 describes the viscoelastic properties of bitumen. Only the phase angle index (I_P) showed a significant correlation with PC2. When the viscoelastic property of bitumen is recovered, the fibril structure becomes a "random" state correspondingly. Further investigation is needed to characterize this phenomenon. Furthermore, the PCA-score plot provides information about the influence of chemical composition on microstructure. The addition of aromatics (Rej-A) mainly enhanced the viscous portion of rheology, and the addition of saturates (Rej—B) reduces the stiffness.

Thirdly, the quantitative relationship between the rheological properties of binders and microstructure parameters was established by the regression analysis method. For instance, the parameter *a* (distance between adjacent fibril) has shown a significant linear positive correlation with $J_{nr3.2}$ ($R^2 = 0.92$) and an exponential negative correlation with I_M ($R^2 = 0.71$), indicating a good connection between ESEM microstructure and rheology.

In summary, the current observations strengthen the hypothesis that the ESEM microstructure is intimately correlated with bitumen's chemical composition and rheological properties rather than just an irrelevant surface phenomenon. The establishment of the chemo-microstructural-mechanical relationship of bituminous binder

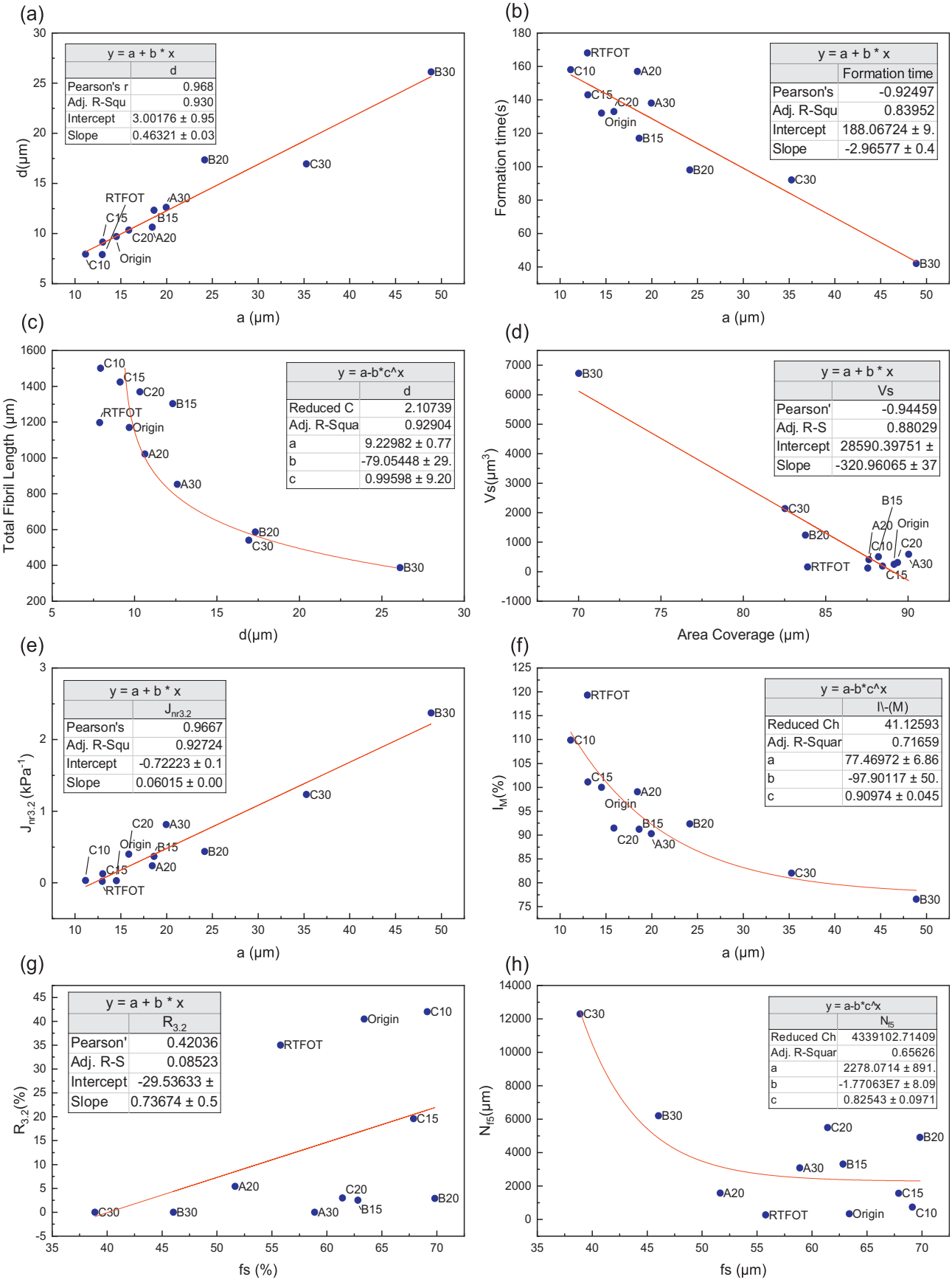

Fig. 16. Correlation between (a-d) microstructure parameters and (e-h) microstructure and rheological parameters.

improves the understanding of the underlying process and mechanism of aging and rejuvenation. This will enable the proper design formula for the rejuvenator or develop an anti-aging agent.

6. Conclusions

In this research, original, aged and rejuvenated SBS modified binders were investigated to establish their chemical, microstructural, and mechanical relationship to reveal the underlying rejuvenation mechanism. Three types of rejuvenators were used to rejuvenate the aged SBS modified bitumen at five different dosages. The rheological properties of binders were measured with DSR. The microstructure of rejuvenated binders was observed with ESEM, and a series of microstructure parameters were extracted. The rheological and microstructure characteristics were analyzed with PCA and regression analysis, and the conclusions are the following:

- Chemical compositional changes of binders correspond with the rheological and microstructure alterations. The saturate fraction increase mainly decreases the binder stiffness, and the corresponding microstructure becomes sparse. Moreover, the addition of aromatic fraction mainly increases the viscous portion, and the corresponding microstructure becomes more random rather than perpendicular. Further addition of the SBS polymer and rejuvenator led to an increase in the viscous portion and made the fibril microstructure visible.
- From PCA results, microstructure and rheological parameters can be combined into two principal components (PC1 and PC2), in which PC1 accounts for the stiffness and PC2 accounts for the viscoelastic property of binders. Among the microstructure parameters obtained from ESEM, fibril structure formation time, total fibril length, fibril diameter and distance between adjacent fibril structure explain the stiffness of binder, and volume density of fibril structure is associated with both stiffness and viscoelastic property.
- According to the regression analysis, the distance between adjacent fibrils exhibited a significant correlation with $J_{nr3.2}$ ($R^2 = 0.92$) and complex modulus index ($R^2 = 0.71$), and the volume density of fibril structure showed a correlation with fatigue life ($R^2 = 0.66$). It strengthens the hypothesis that the microstructure is intimately associated with the binder composition and rheological properties rather than just an irrelevant surface phenomenon.

Credit author statement

The authors confirm contribution to the paper as follows: study conception and design: Xueyan Liu, Peng Lin, Panos Apostolidis, Sandra Erkens; data collection: Peng Lin and Yi Zhang; analysis and interpretation of results: Xueyan Liu, Peng Lin and Panos Apostolidis; draft manuscript preparation: Peng Lin, Xueyan Liu, Panos Apostolidis and Shisong Ren. All authors reviewed the results and approved the final version of the manuscript.

Declaration of Competing Interest

The authors declare that they have no known competing financial interests or personal relationships that could have appeared to influence the work reported in this paper.

Acknowledgments

Special thanks to Laurent Porot (Kraton Polymers BV) for supplying the SBS copolymer and the SBS modified bitumen used in this research. We would like to thank Arjan Thijssen from Microlab Civil Engineering & Geosciences at the Delft University of Technology for ESEM technique and analysis support.

References

[1] Asphalt Institute, European Bitumen Association, The Bitumen Industry: a Global Perspective: Production, Chemistry Use, Specification and Occupational Exposure, 2015.
[2] F. Chaignon, P. Eapa, Asphalt Fig. 2018 (2018) 13.
[3] M. Zaumanis, R.B. Mallick, Review of very high-content reclaimed asphalt use in plant-produced pavements: state of the art, Int. J. Pav. Eng. 16 (2015) 39–55, https://doi.org/10.1080/10298436.2014.893331.
[4] N. Tran, A. Taylor, P. Turner, C. Holmes, L. Porot, Effect of rejuvenator on performance characteristics of high RAP mixture, Road Mater. Pav. Design. 18 (2017) 183–208, https://doi.org/10.1080/14680629.2016.1266757.
[5] R. Tauste, F. Moreno-Navarro, M. Sol-Sánchez, M.C. Rubio-Gámez, Understanding the bitumen ageing phenomenon: a review, Constr. Build. Mater. 192 (2018) 593–609, https://doi.org/10.1016/j.conbuildmat.2018.10.169.
[6] J.C. Petersen, Transportation Research Circular E-C140: A Review of the Fundamentals of Asphalt Oxidation: Chemical, Physicochemical, Physical Property, and Durability Relationships, Transportation Research Board of the National Academies, Washington, DC, 2009.
[7] F. Zhou, P. Karki, Rejuvenator Laboratory Characterization and Field Performance, 2021 218.
[8] W.S. Mogawer, A. Austerman, R. Roque, S. Underwood, L. Mohammad, J. Zou, Ageing and rejuvenators: evaluating their impact on high RAP mixtures fatigue cracking characteristics using advanced mechanistic models and testing methods, Road Mater. Pav. Design. 16 (2015) 1–28, https://doi.org/10.1080/14680629.2015.1076996.
[9] L. Porot, D. Broere, M. Wistuba, J. Grönniger, Asphalt and binder evaluation of asphalt mix with 70% reclaimed asphalt, Road Mater. Pav. Design. 18 (2017) 66–75, https://doi.org/10.1080/14680629.2017.1304259.
[10] J. Shen, S. Amirkhanian, J. Aune Miller, Effects of rejuvenating agents on superpave mixtures containing reclaimed asphalt pavement, J. Mater. Civ. Eng. 19 (2007) 376–384, https://doi.org/10.1061/(ASCE)0899-1561(2007)19:5(376).
[11] J. Shen, S. Amirkhanian, S.-J. Lee, The effects of rejuvenating agents on recycled aged CRM binders, Int. J. Pav. Eng. 6 (2005) 273–279, https://doi.org/10.1080/10298430500439319.
[12] K.-A.N. Johnson, S.A.M. Hesp, Effect of waste engine oil residue on quality and durability of SHRP materials reference library binders, Transp. Res. Rec. 2444 (2014) 102–109, https://doi.org/10.3141/2444-12.
[13] P. Karki, F. Zhou, Effect of rejuvenators on rheological, chemical, and aging properties of asphalt binders containing recycled binders, Transp. Res. Rec. 2574 (2016) 74–82, https://doi.org/10.3141/2574-08.
[14] T. Baghaee Moghaddam, H. Baaj, The use of rejuvenating agents in production of recycled hot mix asphalt: a systematic review, Constr. Build. Mater. 114 (2016) 805–816, https://doi.org/10.1016/j.conbuildmat.2016.04.015.
[15] X. Yu, M. Zaumanis, S. dos Santos, L.D. Poulikakos, Rheological, microscopic, and chemical characterization of the rejuvenating effect on asphalt binders, Fuel. 135 (2014) 162–171, https://doi.org/10.1016/j.fuel.2014.06.038.
[16] D. Ghosh, M. Turos, E. Johnson, M. Marasteanu, Rheological characterization of asphalt binders treated with bio sealants for pavement preservation, Can. J. Civ. Eng. 45 (2018) 407–412, https://doi.org/10.1139/cjce-2017-0058.
[17] M.N. Siddiqui, M.F. Ali, Studies on the aging behavior of the Arabian asphalts, Fuel. 78 (1999) 1005–1015, https://doi.org/10.1016/S0016-2361(99)00018-6.
[18] J. Wang, T. Wang, X. Hou, F. Xiao, Modelling of rheological and chemical properties of asphalt binder considering SARA fraction, Fuel. 238 (2019) 320–330, https://doi.org/10.1016/j.fuel.2018.10.126.
[19] A. Hung, E.H. Fini, Surface morphology and chemical mapping of UV-aged thin films of bitumen, ACS Sustain. Chem. Eng. 8 (2020) 11764–11771, https://doi.org/10.1021/acssuschemeng.0c03877.
[20] A.A. Hussein, R.P. Jaya, N. Abdul Hassan, H. Yaacob, G.F. Huseien, M.H.W. Ibrahim, Performance of nanoceramic powder on the chemical and physical properties of bitumen, Constr. Build. Mater. 156 (2017) 496–505, https://doi.org/10.1016/j.conbuildmat.2017.09.014.
[21] K. Yan, H. Zhang, H. Xu, Effect of polyphosphoric acid on physical properties, chemical composition and morphology of bitumen, Constr. Build. Mater. 47 (2013) 92–98, https://doi.org/10.1016/j.conbuildmat.2013.05.004.
[22] Z.-G. Feng, J.-Y. Yu, H.-L. Zhang, D.-L. Kuang, L.-H. Xue, Effect of ultraviolet aging on rheology, chemistry and morphology of ultraviolet absorber modified bitumen, Mater. Struct. 46 (2013) 1123–1132.
[23] H.L. Zhang, J.Y. Yu, Z.G. Feng, L.H. Xue, S.P. Wu, Effect of aging on the morphology of bitumen by atomic force microscopy, J. Microsc. 246 (2012) 11–19, https://doi.org/10.1111/j.1365-2818.2011.03578.x.
[24] X. Lu, M. Langton, P. Olofsson, P. Redelius, Wax morphology in bitumen, J. Mater. Sci. 40 (2005) 1893–1900.
[25] S. Bearsley, A. Forbes, R.G. Haverkamp, Direct observation of the asphaltene structure in paving-grade bitumen using confocal laser-scanning microscopy, J. Microsc. 215 (2004) 149–155.
[26] D. Sun, G. Sun, X. Zhu, Q. Pang, F. Yu, T. Lin, Identification of wetting and molecular diffusion stages during self-healing process of asphalt binder via fluorescence microscope, Constr. Build. Mater. 132 (2017) 230–239, https://doi.org/10.1016/j.conbuildmat.2016.11.137.
[27] D. Lesueur, The colloidal structure of bitumen: consequences on the rheology and on the mechanisms of bitumen modification, Adv. Colloid Interf. Sci. 145 (2009) 42–82, https://doi.org/10.1016/j.cis.2008.08.011.
[28] F. Handle, J. Füssl, S. Neudl, D. Grossegger, L. Eberhardsteiner, B. Hofko, M. Hospodka, R. Blab, H. Grothe, The bitumen microstructure: a fluorescent approach, Mater. Struct. 49 (2016) 167–180.

[29] R. Jahangir, D. Little, A. Bhasin, Evolution of asphalt binder microstructure due to tensile loading determined using AFM and image analysis techniques, Int. J. Pav. Eng. 16 (2015) 337–349.
[30] A. Jäger, R. Lackner, C. Eisenmenger-Sittner, R. Blab, Identification of microstructural components of bitumen by means of atomic force microscopy (AFM), PAMM: Proceedings in Applied Mathematics and Mechanics, Wiley Online Library 2004, pp. 400–401.
[31] H. Soenen, J. Besamusca, H.R. Fischer, L.D. Poulikakos, J.-P. Planche, P.K. Das, N. Kringos, J.R.A. Grenfell, X. Lu, E. Chailleux, Laboratory investigation of bitumen based on round robin DSC and AFM tests, Mater. Struct. 47 (2014) 1205–1220, https://doi.org/10.1617/s11527-013-0123-4.
[32] J. Stulirova, K. Pospisil, Observation of bitumen microstructure changes using scanning electron microscopy, Road Mater. Pav. Design. 9 (2008) 745–754, https://doi.org/10.1080/14680629.2008.9690148.
[33] K. Pospíšil, A. Frýbort, A. Kratochvíl, J. Macháčková, Scanning electron microscopy method as a tool for the evaluation of selected materials microstructure, Transact. Trans. Sci. 1 (2008) 13–20.
[34] M. Mazumder, R. Ahmed, A. Wajahat Ali, S.-J. Lee, SEM and ESEM techniques used for analysis of asphalt binder and mixture: a state of the art review, Constr. Build. Mater. 186 (2018) 313–329, https://doi.org/10.1016/j.conbuildmat.2018.07.126.
[35] L. Loeber, O. Sutton, J. Morel, J.-M. Valleton, G. Muller, New direct observations of asphalts and asphalt binders by scanning electron microscopy and atomic force microscopy, J. Microsc. 182 (1996) 32–39, https://doi.org/10.1046/j.1365-2818.1996.134416.x.
[36] J.-B. Donnet, J. Ducret, M. Kennel, E. Papirer, Electron microscopic observations of the morphology of bitumens, Fuel. 56 (1977) 97–100.
[37] G.D. Daniatos, Design and construction of an atmospheric or environmental SEM (part 1), Scanning. 4 (1981) 9–20.
[38] G.D. Danilatos, R. Postle, Design and construction of an atmospheric or environmental SEM—2, Micron 14 (1983) (1969) 41–52.
[39] G.D. Danilatos, Design and construction of an atmospheric or environmental SEM (part 3), Scanning. 7 (1985) 26–42.
[40] A.S. Bhurke, E.E. Shin, L.T. Drzal, Fracture morphology and fracture toughness measurement of polymer-modified asphalt concrete, Transp. Res. Rec. 1590 (1997) 23–33, https://doi.org/10.3141/1590-04.
[41] S.J. Rozeveld, E.E. Shin, A. Bhurke, L. France, L.T. Drzal, Network morphology of straight and polymer modified asphalt cements, Microsc. Res. Tech. 38 (1997) 529–543, https://doi.org/10.1002/(SICI)1097-0029(19970901)38:5<529::AID-JEMT11>3.0.CO;2-O.
[42] M.C. Hawley, L.T. Drzal, G. Baladi, Y.-J. Lee, Final Report on Polymers in Bituminous Mixtures - PHASE II, https://trid.trb.org/view/496572 1997. (Accessed 25 June 2020).
[43] K. Stangl, A. Jäger, R. Lackner, Microstructure-based identification of bitumen performance, Road Mater. Pav. Design. 7 (2006) 111–142, https://doi.org/10.1080/14680629.2006.9690061.
[44] L.C. Michon, T.M. Williams, F.P. Miknis, J.-P. Planche, D. Martin, Use of the environmental scanning electron microscope to investigate three polymer modified asphalts, Pet. Sci. Technol. 16 (1998) 797–809, https://doi.org/10.1080/10916469808949812.
[45] J. Gaskin, On Bitumen Microstructure and the Effects of Crack Healing, (Notingham University PhD Thesis) 265.
[46] P. Mikhailenko, H. Kadhim, H. Baaj, Observation of bitumen microstructure oxidation and blending with ESEM, Road Mater. Pav. Design. 18 (2017) 216–225, https://doi.org/10.1080/14680629.2017.1304251.
[47] P. Mikhailenko, C. Kou, H. Baaj, S. Tighe, Observation of Polymer Modified Asphalt Microstructure by ESEM, 2017 11.
[48] P. Mikhailenko, C. Kou, H. Baaj, L. Poulikakos, A. Cannone-Falchetto, J. Besamusca, B. Hofko, Comparison of ESEM and physical properties of virgin and laboratory aged asphalt binders, Fuel. 235 (2019) 627–638, https://doi.org/10.1016/j.fuel.2018.08.052.
[49] J. Zhu, B. Birgisson, N. Kringos, Polymer modification of bitumen: advances and challenges, Eur. Polym. J. 54 (2014) 18–38.
[50] J.C. Munera, E.A. Ossa, Polymer modified bitumen: optimization and selection, Mater. Des. 62 (2014) (1980-2015) 91–97, https://doi.org/10.1016/j.matdes.2014.05.009.
[51] G. Polacco, J. Stastna, D. Biondi, L. Zanzotto, Relation between polymer architecture and nonlinear viscoelastic behavior of modified asphalts, Curr. Opin. Colloid Interface Sci. 11 (2006) 230–245, https://doi.org/10.1016/j.cocis.2006.09.001.
[52] C. Yan, W. Huang, P. Lin, Y. Zhang, Q. Lv, Chemical and rheological evaluation of aging properties of high content SBS polymer modified asphalt, Fuel. 252 (2019) 417–426.
[53] P. Lin, C. Yan, W. Huang, Y. Li, L. Zhou, N. Tang, F. Xiao, Y. Zhang, Q. Lv, Rheological, chemical and aging characteristics of high content polymer modified asphalt, Constr. Build. Mater. 207 (2019) 616–629, https://doi.org/10.1016/j.conbuildmat.2019.02.086.
[54] N.I. Md, F.M. Jakarni Yusoff, V.H. Nguyen, M.R. Hainin, G.D. Airey, Modelling the rheological properties of bituminous binders using mathematical equations, Constr. Build. Mater. 40 (2013) 174–188, https://doi.org/10.1016/j.conbuildmat.2012.09.105.
[55] H.C. Booij, G.P.J.M. Thoone, Generalization of Kramers-Kronig transforms and some approximations of relations between viscoelastic quantities, Rheol. Acta 21 (1982) 15–24, https://doi.org/10.1007/BF01520701.
[56] M. Oshone, E. Dave, J.S. Daniel, G.M. Rowe, Prediction of phase angles from dynamic modulus data and implications for cracking performance evaluation, Road Mater. Pav. Design. 18 (2017) 491–513, https://doi.org/10.1080/14680629.2017.1389086.
[57] M.C. Cavalli, M. Zaumanis, E. Mazza, M.N. Partl, L.D. Poulikakos, Effect of ageing on the mechanical and chemical properties of binder from RAP treated with bio-based rejuvenators, Compos. Part B 141 (2018) 174–181, https://doi.org/10.1016/j.compositesb.2017.12.060.
[58] C. Hintz, R. Velasquez, C. Johnson, H. Bahia, Modification and validation of linear amplitude sweep test for binder fatigue specification, Transp. Res. Rec. 2207 (2011) 99–106, https://doi.org/10.3141/2207-13.
[59] N. Saboo, R. Kumar, P. Kumar, A. Gupta, Ranking the rheological response of SBS- and EVA-modified bitumen using MSCR and LAS tests, J. Mater. Civ. Eng. 30 (2018), 04018165, https://doi.org/10.1061/(ASCE)MT.1943-5533.0002367.
[60] X. Lu, U. Isacsson, Influence of styrene-butadiene-styrene polymer modification on bitumen viscosity, Fuel. 76 (1997) 1353–1359, https://doi.org/10.1016/S0016-2361(97)00144-0.
[61] G.D. Airey, Rheological properties of styrene butadiene styrene polymer modified road bitumens, Fuel. 82 (2003) 1709–1719, https://doi.org/10.1016/S0016-2361(03)00146-7.
[62] Peng Lin, Huang Weidong, Liu Xueyan, Apostolids Panos, Haopeng Wang, Yan Chuanqi, Laboratory evaluation of the effects of long-term aging on high-content polymer-modified asphalt binder, J. Mater. Civ. Eng. 32 (2020), 04020157, https://doi.org/10.1061/(ASCE)MT.1943-5533.0003208.
[63] M. Dirand, V. Chevallier, E. Provost, M. Bouroukba, D. Petitjean, Multicomponent paraffin waxes and petroleum solid deposits: structural and thermodynamic state, Fuel. 77 (1998) 1253–1260, https://doi.org/10.1016/S0016-2361(98)00032-5.
[64] X. Lu, P. Sjövall, H. Soenen, M. Andersson, Microstructures of bitumen observed by environmental scanning electron microscopy (ESEM) and chemical analysis using time-of-flight secondary ion mass spectrometry (TOF-SIMS), Fuel. 229 (2018) 198–208, https://doi.org/10.1016/j.fuel.2018.05.036.
[65] P. Mikhailenko, H. Kadhim, H. Baaj, Observation of bitumen microstructure oxidation and blending with ESEM, Road Mater. Pav. Design. 18 (2017) 216–225, https://doi.org/10.1080/14680629.2017.1304251.
[66] I.T. Jolliffe, Principal Component Analysis, Springer New York, NY, 2002.
[67] A. Margaritis, H. Soenen, E. Fransen, G. Pipintakos, G. Jacobs, J. Blom, W. Van Den Bergh, Identification of ageing state clusters of reclaimed asphalt binders using principal component analysis (PCA) and hierarchical cluster analysis (HCA) based on chemo-rheological parameters, Constr. Build. Mater. 244 (2020) 118276, https://doi.org/10.1016/j.conbuildmat.2020.118276.
[68] W.J. Halstead, Relation of Asphalt Chemistry to Physical Properties and Specifications, Virginia Transportation Research Council, 1984.
[69] X. Yu, N.A. Burnham, S. Granados-Focil, M. Tao, Bitumen's microstructures are correlated with its bulk thermal and rheological properties, Fuel. 254 (2019) 115509, https://doi.org/10.1016/j.fuel.2019.05.092.
[70] P. Redelius, H. Soenen, Relation between bitumen chemistry and performance, Fuel. 140 (2015) 34–43.